1994

A Degenerate Four-Wave Mixing Study Of Third-Order Optical Nonlinearity Of Transition Metal Containing Organic Complexes.

Tianyi Zhai
University of Alabama at Birmingham

Order Number 9425332

A degenerate four-wave mixing study of third-order optical nonlinearity of transition metal containing organic complexes

Zhai, Tianyi, Ph.D.

University of Alabama at Birmingham, 1994

U·M·I
300 N. Zeeb Rd.
Ann Arbor, MI 48106

A DEGENERATE FOUR-WAVE MIXING STUDY OF THIRD-ORDER OPTICAL NONLINEARITY OF TRANSITION METAL CONTAINING ORGANIC COMPLEXES

by

TIANYI ZHAI

A DISSERTATION

Submitted in partial fulfillment of the requirement for the degree of
Doctor of Philosophy in the Department of Physics
in the Graduate School, The University of
Alabama at Birmingham

BIRMINGHAM, ALABAMA

1994

ABSTRACT OF DISSERTATION
GRADUATE SCHOOL, UNIVERSITY OF ALABAMA AT BIRMINGHAM

Degree Ph. D. Major Subject Physics

Name of Candidate Tianyi Zhai

Title A Degenerate Four-wave Mixing Study of Third-order Optical Nonlinearity of Transition Metal Containing Organic Complexes

All-optical devices play a major role in acquiring, storing, transmitting, and processing information rapidly. Transition metal-based organic complexes are prospective materials for these kinds of devices. These metal-organic materials have a number of advantages over conventional nonlinear optical materials such as: ultrafast response time, the ability to engineer molecular structure, and a high laser damage threshold.

A backward degenerate four-wave mixing apparatus has been built to measure the properties of metal-organic complexes. The light source is a Nd:YAG Pockels' cell Q-switched pulse laser. The output energy of the laser is approximately 7 mJ when operated at a rate of 2 pps. The laser pulse duration is 20 nS, and the fundamental lasing wavelength is 1064 nm. The output intensity variation of the laser is about of 3%. The Nd:YAG laser is frequency doubled using a KDP (potassium dihydrogen phosphate, KH_2PO_4) crystal so that 532 nm pulses are used for the degenerate four-wave mixing experiment.

The third-order nonlinear optical property for samples of molybdenum (Mo), palladium (Pd), platinum (Pt), rhodium (Rh), and tungsten (W) complexes has been measured by the degenerate four-wave mixing technique. Most of the complexes have a molecular structure of $C \equiv O$ and phosphine ligands coordinated on the metal atom. The experimentally measured second-order molecular hyperpolarizabilities range from

$\gamma = 1.9 \times 10^{-31}$ esu for *cis*-$Pt(CO)_2(PPh_2thiophene)_2$ and $\gamma = 1.7 \times 10^{-31}$esu for *cis*-$Mo(CO)_4(PPh_3)_2$ to $\gamma = 1.5 \times 10^{-34}$esu for $Mo(CO)_5(PPh_3)$ and $\gamma = 1.7 \times 10^{-34}$ esu for $Rh(CO)_2(acac)$. The results indicate that the nonlinear optical mechanisms that lead to these γ values are nonresonant.

Analysis shows that the electron donor/acceptor ability of the substituents on phosphine ligands does not affect the mono(phosphine) Mo complex's third-order nonlinear optical response at all, while its effect on the bis(phosphine) complex is limited. The major factor that dramatically enhances second-order molecular hyperpolarizability is the π electron structure of the substituentson in the phosphine ligands. It has been found that the larger the number of the substituents of a π-electron structure on phosphine ligands, the larger the observed third-order nonlinearity. For molybdenum complexes, the magnitude of the second-order molecular hyperpolarizability, γ, increases approximately as the 5th power of the number of substituents having a π-electron structure. It is also observed that for the complexes with the same type phosphine ligand, the cis-type complexes yield a larger γ value than that of the complexes with the trans-type coordination geometry.

The charge transfer is probably through the ligand-to-ligand mechanism rather than through the ligand-to-metal-to-ligand mechanism. The type of metal does affect the measured second-order molecular hyperpolarizability. Complexes with a metal of second row of the periodic table exhibit a larger γ value, though the effect of the metal is not as drastic as that of the π electron structure substituents on ligands.

Abstract Approved by: Committee Chairman Chris M. Lawson

Program Director

Date 4/7/94 Dean of Graduate School

PS-5744

DEDICATION

To my parents, Panchan and Xiaoqiao,

for their lifetime of selfless support and encouragement.

ACKNOWLEDGMENTS

I wish to thank Dr. Chris Lawson, Chair of my Graduate Committee. I am also in debt to Dr. John Young, who has helped me a lot in writing the dissertation. Special appreciation goes to Dr. Gary Gray for helping me to choose the research subject and spending enormous time teaching me about organometallics; without him, there would have been no dissertation.

I wish to express my gratitude to Dr. Joseph Harrison and Dr. Jimmy Mays for serving on my academic committee. I would like to acknowledge the Graduate School for the financial support of my graduate program.

I wish to thank Dr. David Shealy, Chair of the Department and Director of the Graduate Program. It was his support throughout my study that made the work here possible.

I would like to thank my fellow graduate students Mr. Guy Burgess and Mr. David Gale for their beneficial discussions.

My thanks also go to other faculty members of the Department of Physics for their direct or indirect help during my study. I would like to thank Dr. Michael Lewis for his help in setting up the experiment. I would like to thank Mr. Jerry Sewell and Mr. Minghuan Shen, who contributed a lot to the research. My gratitude extends also to Ms. Donna Hamer and Ms. Donna Andrews.

Finally, I want to say to my wife and child, Xiaoying and Yujia, thank you for supporting me unconditionally all the time.

TABLE OF CONTENTS

TABLE OF CONTENTS (Continued)

LIST OF TABLES

LIST OF FIGURES

LIST OF FIGURES (Continued)

CHAPTER 1

INTRODUCTION

During recent years, there has been increasing interest in the area of nonlinear optical phenomena. More researchers are involved in the study and development of nonlinear optics, and the amount of the related information has increased rapidly. These research and development activities are motivated by the prospect that nonlinear optics will play a major role in communication, computation, and signal storing and processing areas.

There has emerged the terminology *photonics* as the analog of electronics in describing the nonlinear optics based functions in acquiring, storing, transmitting, and processing information by using photons instead of electrons. It is quite natural for people to turn their attention to the optical domain while continuing the efforts of extracting the remaining capability from electronics to fulfill the increasing demand for higher speed communication, computation, and controlling.

1.1 The Development of Nonlinear Optics

It is generally accepted that nonlinear optics emerged three decades ago when the laser provided the necessary tool that enabled people to observe nonlinear optical phenomena. The landmark of modern nonlinear optics was laid down by Franken[1] and his colleagues through their discovery of the second harmonic generation from a quartz crystal upon which a ruby laser at the wavelength of 694.2 nm impinged. The observed frequency-doubled output of the light at 347.1 nm excited researchers worldwide since it proved that the same phenomenon found in the low-frequency electromagnetic wave

domain also could be realized in the high-frequency domain, which had been suspected for a long time. A door was then opened to a totally new region.

Following Franken's discovery, a number of experimental results were reported on subjects such as phase matching in birefringence,[2] two-photon absorption,[3] and many other nonlinear optical phenomena.[4-6] During the 1960s, most research was concentrated in second-order phenomena and inorganic materials such as lithium niobate ($LiNbO_3$), potassium dihygrogen phosphate (KH_2PO_4, usually called KDP), and gallium arsenic (GaAs). These materials have a large second-order susceptibility; therefore the second harmonic generation efficiency is high. In addition, they have been used in devices for frequency mixters, parameter processors, and electro-optic modulators.

Since 1970s more researchers have entered the field dealing with higher order nonlinear optical phenomena, while searches for better nonlinear optical materials were extended to include organic systems. Particularly since the late 1980s, optical fiber has been adopted rapidly as the major means of transferring information in communication, and the optical storage technique showed its capacity in the information storage industry. The demands for faster and better optical nonlinear devices have had a huge impact on developing inorganic as well as organic materials.

Nonlinear optics involves a class of interaction between an optical wave and medium in a way that is not the same as in linear phenomena. In describing the medium response to an optical wave the polarization is crucial. While the linear polarization depends on the first power of optical field strength, the higher order nonlinear polarizations may depend on the second, third, or even higher powers of the optical field strength for nonlinear processes. We can generally express medium polarization $\vec{\mathbf{P}}$ as the sum of the linear and nonlinear terms:

$$\begin{aligned}\vec{\mathbf{P}} &= \vec{\mathbf{P}}^{L} + \vec{\mathbf{P}}^{(2)} + \vec{\mathbf{P}}^{(3)} + \cdots \\ &= \chi^{(1)} \cdot \vec{\mathbf{E}} + \chi^{(2)} : \vec{\mathbf{E}}\vec{\mathbf{E}} + \chi^{(3)} : \vec{\mathbf{E}}\vec{\mathbf{E}}\vec{\mathbf{E}} + \cdots,\end{aligned} \tag{1.1}$$

or in microscopic terms

$$\vec{p} = \alpha \cdot \vec{E} + \beta : \vec{E}\vec{E} + \gamma \vdots \vec{E}\vec{E}\vec{E} + \cdots . \tag{1.2}$$

Here, $\vec{P}^{L}$, $\vec{P}^{(2)}$, and $\vec{P}^{(3)}$ represent the linear, second-, and third-order polarizations; the coefficients $\chi^{(1)}$, $\chi^{(2)}$, and $\chi^{(3)}$ are called linear, second-, and third-order susceptibilities. $\vec{p}$ is the polarization for an individual molecule, and α, β, and γ are the counterparts of χs in the microscopic domain and are called the linear, first-order and second-order molecular hyperpolarizabilities, respectively.

As a matter of fact, all media respond to the optical field nonlinearly. Just like the situation of treating the spring oscillator in classic mechanics, the linear descriptions are only an approximation toward the actual nonlinear process. Usually, the nonlinear susceptibilities $\chi^{(2)}$ and $\chi^{(3)}$ are small. Without an intense optical field, the nonlinear polarizations are too weak to be observable. That is why it was only after the invention of the laser that nonlinear optics research had shown progress, even though the Pockels, Kerr, and Faraday effects were discovered a long time ago.

In addition to causing new, nonlinear optic effects, the nonlinear terms, $\vec{P}^{(2)}$ and $\vec{P}^{(3)}$, bring additional complexity into the already complicated situation of describing electromagnetic waves within a medium. This is especially true because of the tensor nature of $\vec{P}^{(2)}$ and $\vec{P}^{(3)}$. Individual tensor elements may respond to the various incident optical wave configurations in different ways. Therefore, the comparison among reported nonlinear optical properties has to be made in accordance with the methods involved.

The response of a medium to the incident optical wave can be roughly described as the electrons and ions within the medium reacting to the optical field such that a group of dipoles is generated; the newly generated dipoles oscillate and emit electromagnetic waves that in turn affect the propagation of the original optical wave. If the original incident optical wave is not intense enough or the dipoles harmonic range is large, little nonlinear effect will show. If the optical wave has a high intensity or the dipole oscillator has a tiny

harmonic range, the response of the dipole will yield a nonlinear effect of an anharmonic oscillator. It is this anharmonic oscillator's characteristic that determines the nonlinear susceptibilities. The anharmonic oscillator model was used by Bloembergen[7] to establish the formula for second- and third-order nonlinear susceptibilities of dielectric materials. There is another free-electron model that deals with relatively free-moving charge carriers.

1.2 Potential NLO Applications

Nonlinear optical processes may consist of two parts. The intense light first induces a nonlinear response in the medium, and then the medium in reacting modifies the incident optical field in a nonlinear way. The possible applications can then be divided into two categories: one acts as a probe technique to study material properties, and another makes use of the modified optical field to perform certain tasks similar to what the transistor does in electronics. Some examples of the possible applications in the device area will be briefly presented here.

The concept of employing the medium's nonlinear response to an optical field as an optical device emerges immediately after Franken's discovery.

Frequency conversion is the one that utilizes the harmonic generation to change laser output frequency. In optical storage, the surface information storage efficiency is inversely proportional to the square of the light spot diameter. The theoretical limitation on the light spot size, or the resolution of a lens, is[41]

$$R = 0.61\lambda / n \sin\theta, \tag{1.3}$$

where n is the index of refraction, θ is determined by the relative orientation of the light with the surface, and λ is the wavelength of laser light. Doubling a diode laser frequency, and hence cutting the wavelength in half, the storage density will go up four-fold. The same frequency conversion technique is used in tuning the powerful laser output. Materials for frequency-doubling devices are $LiNbO_3$, KDP, and ADP.

For devices using the third-order nonlinear effects, most of them are based on the fact that the index of refraction, n, of the medium is a function of the incident light intensity I. The relationship is[8]

$$n = n_0 + \frac{a}{n_0}\chi^{(3)} \cdot I. \tag{1.4}$$

This relation is based on the assumptions that the magnetic effect can be ignored and no second-order process is involved.

Optical switching can be achieved by using a waveguide made of materials with a large third-order susceptibility, $\chi^{(3)}$. A schematic representation of this process is shown in Figure 1.1 (a). The evanescent coupling between two very close waveguides is dependent on the intensity-dependent index of refraction. The change of light intensity in one channel will affect the light propagation parameters in the adjacent channel through the coupling. The properly tuned coupling parameters will result in the controlling of the "on" or "off " state for the light in one channel by the light in the other channel.

Optical bistability is another nonlinear optical phenomenon that is similar to what happens in electronics and can be used as a total optical switch or logic device.[9] The principle of such a device is that when a nonlinear optical medium is between two parallel mirrors, the passage of light through the two-mirror device is determined by the resonance condition $2nd = p\lambda$, with n is the index of refraction for the medium, d is the mirror separation, and p is an integer number. When the light intensity increases to a level at which the changed value of the index of refraction satisfies the resonance condition, the maximum light transmission occurs and the device is in the "on" state. After the device is on, even if the incident light intensity decreases a little, the optical field intensity within the medium is still high enough to maintain a large n and the resonant condition continues to be satisfied. The device thus stays "on." When the incident optical field drops to a certain level, the device will return to low transmission and is in the "off" state. This Faby-Perot type behavior is shown in Figure 1.1 (b).

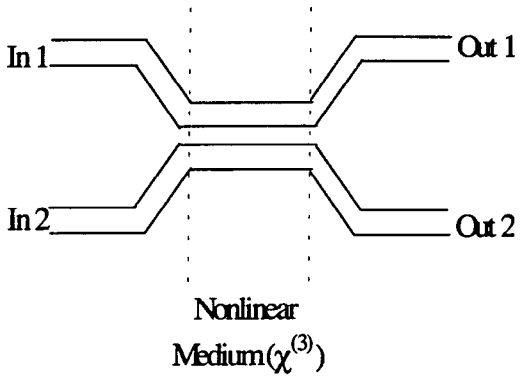

(a) Two-channel Optical Switch

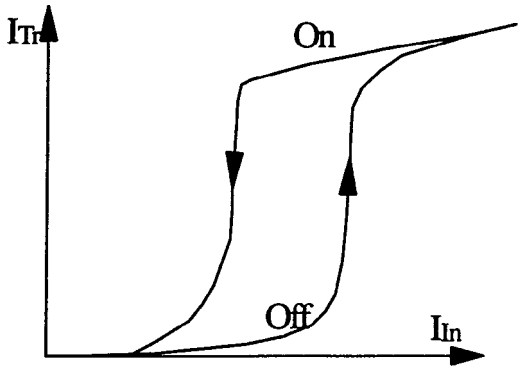

(b) Faby-Perot Optical Bistability

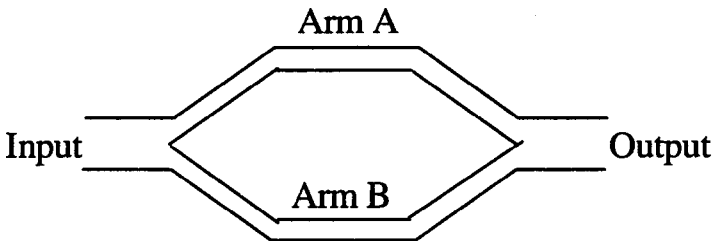

(c) A Mach-Zehnder Interferometer

Figure 1.1 Schematics for some nonlinear optical applications

Though the optical bistability can be utilized in an interferometer,[10] the Mach-Zehnder interferometer shows most clearly how to make use of the nonlinear effect. As can be seen in Figure 1.1 (c), a Mach-Zehnder interferometer consists of two arms that are connected at both ends. If one arm is made of a nonlinear medium with its index of refraction depending on light intensity and the other arm is made of a linear medium, the change in the light intensity in the nonlinear arm will cause a phase shift of the light passing through it and brings about a phase difference between two light beams at the end where they meet. The recombined beam intensity will then be modulated due to the phase difference and can be adjusted at will by changing the intensity of the light that goes through the arm filled with the nonlinear medium.

Image reconstruction and optical distortion correction are other areas where nonlinear optics can make a contribution. The technique utilizes the phase conjugate concept in which a medium of large third-order susceptibility, $\chi^{(3)}$, acts as a mirror. From this mirror the incident light wave is reflected, and the reflected wave will retrace the path of the incident light. This reflected light wave will keep all of the incident light's characteristics but will have a reversed phase. Unlike an ordinary linear mirror, the phase conjugate mirror reserves the wavefront of the incident light wave. The difference between the reflections from an ordinary and a phase conjugate mirror is shown in Figure 1.2. An example of the applications of the phase conjugate mirror is the correction of the laser beam profile distortion caused by an imperfect laser amplifier system.[11]

Sensor protection catches researchers' attention because of the increasing use of the laser. There are many ways to achieve the desired objectives.[12,13] Self-focusing and self-defocusing certainly are the nonlinear processes first considered. Under intensive light, the changes in the index of refraction of the protection medium will automatically cause a shift in the focus position, while the medium appears as transparent to the light at low intensity. Optical switching also can be used to turn off an intense light; with a little modification, the switch can be changed to an optical limiter that allows only a certain

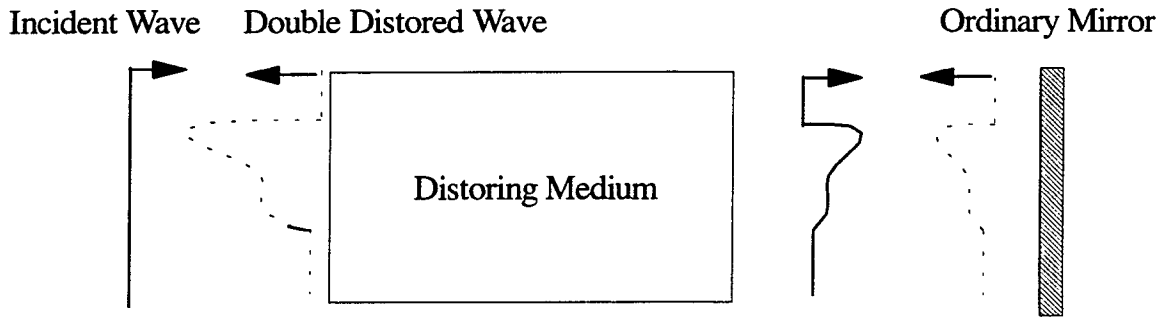

(a) Reflection from an ordinary mirror enlarges the distortion caused by the medium.

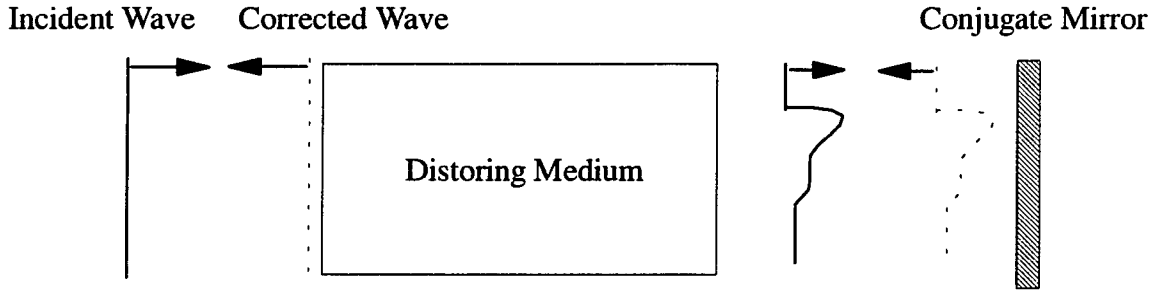

(b) Reflection from a conjugate mirror corrects the distortion caused by the medium.

Figure 1.2 Wavefront correction by the reflection of a conjugate mirror

amount of light to go through. Novel concepts of sensor protection include a combination of alternating layers of linear and nonlinear media. The device is tuned away from Bragg reflection when the incident light is weak. When the light is intense, the changed index of refraction of the nonlinear medium will tune the combination of layers to satisfy the Bragg reflection and the light is reflected away from the sensor, avoiding possible damage to the sensor.

1.3 Nonlinear Optical Materials

Most of the potential applications mentioned above require the medium to have a large third-order susceptibility, $\chi^{(3)}$.

Semiconductors are among the earliest nonlinear optical materials studied. The techniques most widely used in research on $\chi^{(3)}$ materials are third harmonic generation (THG), degenerate four-wave mixing (DFWM), self-action, and two-photon absorption. All of these are due to the nonlinear third-order optical process but differ in the experimental arrangement and thus access different $\chi^{(3)}$ tensor elements, or the combination of the tensor elements.

The theoretical work on the property-structure relations for nonlinear media was first done by Armstrong, et al.[14,15] They used both anharmonic oscillator and free electron gas models. Their research results have provided the guidance for later experiments on semiconductors, since semiconductors have both bound-electron states and free-moving charge carrier states, which are similar to the anharmonic oscillator and free electron gas models, respectively.

The $\chi^{(3)}$ value of the order of 10^{-10} esu for GaAs by using degenerate four-wave mixing was reported in 1966.[16] In 1980s, $\chi^{(3)}$ values as high as 10^{-1} esu, for InSb and HgCdTe, were published.[17] However, semiconductors have disadvantages such as low light-damage threshold (~ 10 Mw/cm^2) and poor optical quality.[18] The major drawback for semiconductor materials is their slow relaxation time that originates from the band-gap electronic structures. Large $\chi^{(3)}$ value, which people wanted, usually comes with an

extremely long free carrier life time of 10^{-7}~10^{-6} seconds because of the real transitions between valance and conduction bands.

The search for materials of large third-order susceptibility and fast reaction time turned to a new direction when a group of Soviet scientists led by Davydov found large second-order susceptibility $\chi^{(2)}$ from benzene on which electron-donor and acceptor groups were attached.[79]

Since Davydov's discovery, organic materials have been suggested as a possible substitution for inorganic materials for applications in nonlinear third-order optics. The first systematic study of organic materials was conducted by Hermann, et al.[19] However, the most important work in organic systems was done by Rustagi and Dueuing,[20] who related the measured third-order nonlinear optical property to π electron conjugation of the organic system. So far, it is believed that large nonlinearities of organic materials are mainly caused by the behavior of π electrons in the system.[21]

The magic of organic systems comes from the versatile bonding of carbon atoms with other atoms. The ground state of carbon is $1s^2 2s^2 2p_x^1 2p_y^1$. A carbon atom can be bonded to another carbon atom through either one, two, or three bonds depending on the environment, since the carbon atom can form four sp^3, three sp^2, or two sp hybrid orbitals. The examples of three bonding situations for single, double, and triple bonding between carbon atoms are shown in Figure 1.3.[22]

When there is a single bond between two carbon atoms, the electron orbitals are overlapped along x-axis which is the axis connecting two carbon atom cores. The electrons involved in this direct overlapping are called σ electrons, and the bond is called σ bond. If all four valence electrons of a carbon atom are in σ bond, the structure is said to be saturated.

An interesting thing happens when two or three bonds between two carbon atoms occurs: there is only one σ bond allowed. The extra electron orbitals are overlapped either along y-axis or z-axis for the double-bond case, and both y-axis and z-axis for the

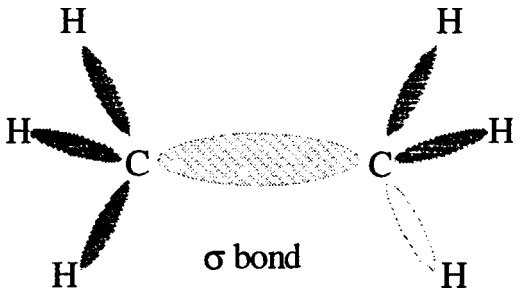

(a) Single σ bond between C atoms

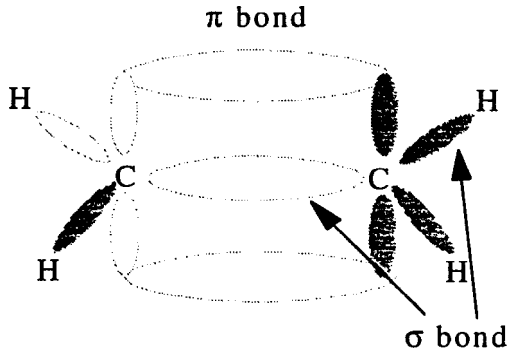

(b) Double-bond between C atoms

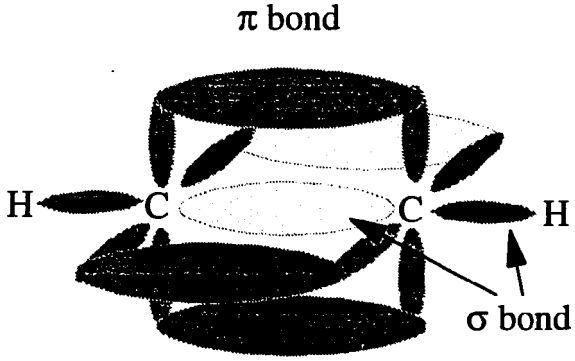

(c) Triple-bond between C atoms

Figure 1.3 The schematics of single, double, and triple bonding between carbon atoms

triple bonds, as shown in Figure 1.3 (b) and (c). These indirectly coupled (not along the axis connecting two carbon atom cores) electrons are called π electrons, and the bonds are called π bond. The rule is that whenever a carbon atom forms a multibond with other atoms only one bond is the σ bond.

The overlaps of π electron orbitals are much weaker than that of σ electrons. This means π electrons are more mobile than σ electrons and tend to form the single bond with other atoms. Thus the carbon multibond structure is called an unsaturated structure. A type of unique structure for carbon atoms is that a σ bond and a π bond are alternately connected together. An example of this type molecule is the benzene ring. In the benzene molecule, every carbon atom is in the same state, and the double bond could be on either side of a carbon atom as long as the other side is a single bond. It is equivalent to saying that π electrons can move over the entire length of the molecule. This type of structure is called a conjugated structure.

In an organic conjugated system, due to the possible large π electron delocalization under the influence of a strong optical field, the electronic dipole could be bigger and, in turn, will yield a larger third-order nonlinear susceptibility. This is based on the assumption that only electric dipoles contribute significantly to the nonlinear optical response. In the sense of increasing π electron delocalization, organic polymers are the natural candidates. Polymers have a length adjustable backbone along which π electrons can move. The polymer backbone unit can be repeated for a very large number. Therefore, the delocalization of π electrons supplied by the side groups attached on the backbone is possibly large as well.

Theoretical calculations suggest that $\chi^{(3)}$ values should increase as the fifth to sixth power of the π electron conjugate length by using the free electron gases model, and three and half power according to ab initio calculation.[20,23] Experimental results report a fourth power by means of third harmonic generation.[24] At the present time, polymers with a $\chi^{(3)}$

value of $\sim 10^{-10}$ esu are not rare. Even a value of 2.7×10^{-7} esu for PBTBQ has been published,[25] and a new technique, excited-state enhancement of the forward type degenerate four-way mixing , is expected to boost the current $\chi^{(3)}$ value by several orders of magnitude.[26]

In designing polymers of a large $\chi^{(3)}$ value, much emphasis is placed on finding those molecular side groups that can enhance the third-order nonlinearity. According to the structures, these side groups can be conjugate in one or two dimensions. In the former, side groups function like a rich π electron reservoir that supplies π electrons to be delocalized along the polymer backbone. For the latter, π electrons can delocalize within the side group in addition to participating in the nonlinear activities along the backbone. Considering the tensor form of the third-order susceptibility $\chi^{(3)}$ and the many ways of aligning the incident optical field polarizations, the added π electron delocalization within the side groups could enhance the macroscopic effective third-order nonlinear optical susceptibility.

Introducing transition metals into organic systems is another way of trying to design materials with a large $\chi^{(3)}$ value. For transition metals, the (n-1)d, ns, and np orbitals must all be regarded as regular valence orbitals.[27] Partial occupation of these orbitals gives transition metals both electron-donor and electron-acceptor properties, depending on what kinds of ligands are bonded to it. The charge transfer caused by coordinating electron-donor/acceptor ligands to a transition metal atom may help to build up a large electric dipole within a compound. On the other hand, due to transition metals' rich low-lying d orbitals, some conjugated organic ligands could have their π electron orbitals overlapping across the "bridge" transition metal atom. This would greatly extend the ligand's π electron delocalization over the whole molecular structure and make it much easier for the π electrons in the side group to delocalize to the polymer backbone structure.

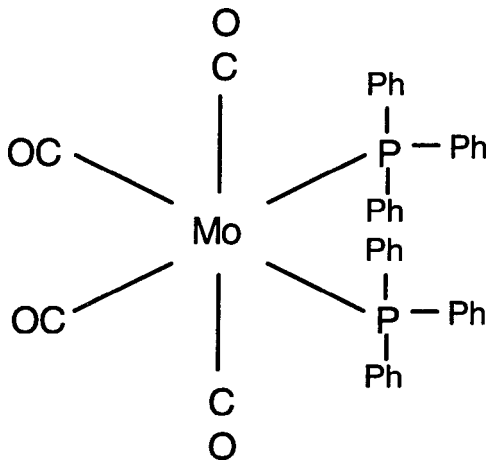

(a) Sandwich type. Ligands attached to the metal atom have their own conjugate structure.

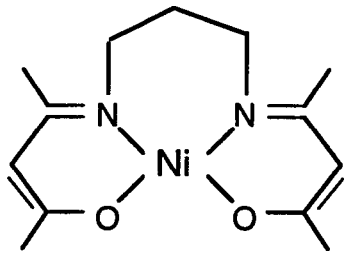

(b) Macrocycle type. Metal atom is a part of the conjugate structure.

Figure 1.4 Two examples of transition metal atoms containing organic complexes

There are many types of organometallic structures. One has a sandwich-like structure, where the transition metal atom is coordinated by a group of ligands that may have their own independent conjugated structures. As illustrated in Figure 1.4 (a), a molybdenum atom is bonded to four CO and two phosphine (PPh_3) ligands. Phenyl itself has a conjugated structure, and phosphine is a good electron-donor. The presence of the phosphine ligands will lead to an increase in the electron density at molybdenum atoms. The combined effect could yield a $\chi^{(3)}$ value larger than the simple summation of the $\chi^{(3)}$ value of the benzene molecules. A $\chi^{(3)}$ value of as large as $\sim 10^{-12}$ esu has been reported for the sandwich-type metal organic system (not the one shown).[28]

In another type of organometallic materials, the transition metal atom is located at the center of a ligand. The ligand itself could be a two-dimensional conjugated system. These structures are sometimes called macrocycles. An example of a macrocycle is shown in Figure 1.4 (b).[80] The metal atom here mainly introduces low-lying energy states derived from metal-to-ligand and ligand-to-metal electron transfer. The system may also present π -π^* resonance, at some wavelengths, that will significantly enhance the measured nonlinear third-order susceptibility. Lindle, et al. have reported a $\chi^{(3)}$ value of $\sim 10^{-9}$ esu for phthalocyanine($ScPc_2$),[29] which has a similar molecular structure to that shown in Figure 1.4 (b).

1.4 General Requirements of Nonlinear Optics Materials

The basic requirements for nonlinear third-order materials are large third-order susceptibility, fast response time, and low absorption at the laser wavelength.[30,31]

As we already know, for the third-order devices, the nonlinear function is achieved through the change of the index of refraction, which depends on the third-order susceptibility $\chi^{(3)}$ and the optical field strength. To have an efficient device, a medium with a bulk property parameter of the second-order index of refraction, $n^{(2)}$, much larger than 10^{-15} m^2/W is needed for all-optical signal processing. In terms of susceptibility, the

$\chi^{(3)}$ value should be larger than 10^{-9} esu. An electro-optic coefficient, r, larger than 30 pm/V is required for electro-optic devices.

A low dielectric constant is required, $\varepsilon \sim 3$, which ensures that the electric-optic device can work at high frequency (~ 10 GHz).

Because many nonlinear optical applications are in the waveguide form, a low loss of less than 1 dB/cm is also required. At the same time, an optical damage threshold of 10 GW/cm^2 is necessary for the materials. Thus the medium's nonlinear response should be the nonresonant, pure electronic process.

All the requirements above must be simultaneously achieved at certain laser wavelengths, preferably at 0.85 μm, 1.3 μm, and 1.55 μm. The materials for the devices should also have good stability in a high-temperature environment The life time for a device should be longer than 5 to 10 years.

Much research needs to be done before metal organic materials can be utilized in nonlinear optical applications. We need a better understanding of how the molecular electronic structure affects the third-order optical response. So far, no theory can explain the origin of nonlinear optical phenomenon without approximation. Better models need to be established, and more experimental data are needed to verify new theories.

CHAPTER 2

THEORY OF DEGENERATE FOUR-WAVE MIXING

2.1. Definitions of Nonlinear Terms

The set of four equations, known as the macroscopic Maxwell equations,

$$\nabla \cdot \vec{\mathbf{D}} = 4\pi\rho \tag{2.1}$$

$$\nabla \cdot \vec{\mathbf{B}} = 0 \tag{2.2}$$

$$\nabla \times \vec{\mathbf{H}} = \frac{4\pi}{c}\vec{\mathbf{J}} + \frac{1}{c}\frac{\partial \vec{\mathbf{D}}}{\partial t} \tag{2.3}$$

$$\nabla \times \vec{\mathbf{E}} = -\frac{1}{c}\frac{\partial \vec{\mathbf{B}}}{\partial t}, \tag{2.4}$$

are the basis of solving all electromagnetic problems, including light traveling inside media. $\vec{\mathbf{E}}$, $\vec{\mathbf{D}}$, $\vec{\mathbf{H}}$ and $\vec{\mathbf{B}}$ are the usual electric and magnetic vectors associated with the light, and $\vec{\mathbf{J}}$ is the conduction current; $\vec{\mathbf{D}}$ and $\vec{\mathbf{H}}$ are related to $\vec{\mathbf{E}}$ and $\vec{\mathbf{B}}$ through the relations

$$\vec{\mathbf{D}} = \vec{\mathbf{E}} + 4\pi\vec{\mathbf{P}} \tag{2.5}$$

$$\vec{\mathbf{H}} = \vec{\mathbf{B}} - 4\pi\vec{\mathbf{M}}. \tag{2.6}$$

Here $\vec{\mathbf{P}}$ is the generalized electric polarization, and $\vec{\mathbf{M}}$ is the magnetization. They both describe the response of the medium to the electromagnetic field. Media of interest in nonlinear optical studies, the present case included, tends to be nonmagnetizable, which means $\vec{\mathbf{M}} \equiv 0$.

In a non-conducting medium, $\vec{\mathbf{J}} = 0$, and substitution of Eqs. (5) and (6) into Eqs. (3) and (4) gives an equation for the electrical field of the light wave in terms of electrical polarization:

$$\nabla^2\vec{\mathbf{E}} - \frac{(n_0)^2}{c^2}\frac{\partial^2\vec{\mathbf{E}}}{\partial t^2} = \frac{4\pi}{c^2}\frac{\partial^2\vec{\mathbf{P}}}{\partial t^2} \tag{2.7}$$

with n_0 being the linear index of refraction.

If the right-hand side is set equal to zero, Eq. (2.7) is the equation describing an electromagnetic wave traveling in free space (vacuum). Hence, it is clear that $\vec{\mathbf{P}}$, the electrical polarization, is the medium response to the light wave, and this $\vec{\mathbf{P}}$ will modify the way the original incident wave travels inside the medium.

To determine the polarization, $\vec{\mathbf{P}}$, solutions of a complicated set of differential equations that describe the interaction of the field with all the individual charges in the medium are needed. To make the picture simple, we can expand the electric potential in terms of the spherical harmonic[32]:

$$\Phi(\vec{\mathbf{r}}) = \sum_{l=0}^{\infty} \sum_{m=-l}^{l} \frac{4\pi}{2l+1} q_{lm} \frac{Y_{lm}(\theta, \phi)}{r^{l+1}}. \tag{2.8}$$

Correspondingly, the polarization $\vec{\mathbf{P}}$ can also be expanded in terms of multipole moments of the charge distribution in the medium[33]:

$$\vec{\mathbf{P}}(\vec{\mathbf{r}}, t) = \vec{\mathbf{p}}(\vec{\mathbf{r}}, t) + \nabla : Q(\vec{\mathbf{r}}, t) + \nabla \vdots O(\vec{\mathbf{r}}, t) + \cdots. \tag{2.9}$$

Here, $\vec{\mathbf{p}}(\vec{\mathbf{r}}, t)$ is the dipole polarization, while $Q(\vec{\mathbf{r}}, t)$ and $O(\vec{\mathbf{r}}, t)$ are the quadrupole and the octupole polarization, respectively.

In most situations, the wavelength of laser radiation (532 nm in our experiment) is much larger than the characteristic dimensions of the molecular oscillations in the medium (typically of the order of 10^{-4} nm), and the $\vec{\mathbf{P}}(\vec{\mathbf{r}}, t)$ expansion converges vary rapidly. We can then retain only the dipole term and omit the quadrupole and higher order terms in the $\vec{\mathbf{P}}$ expansion series. Therefore, only dipole contributions will be considered.

Generally speaking, $\vec{\mathbf{P}}$ is a non-local function of the optical field $\vec{\mathbf{E}}$. Considering that in most cases the laser light fields are weak when compared to the bonding field inside the medium, we can expand the polarization $\vec{\mathbf{P}}$ as a function of the power of the optical field $\vec{\mathbf{E}}$:[35]

$$\vec{P}(\vec{r},\ t) = \int_{-\infty}^{\infty} \chi^{(1)}(\vec{r}-\vec{r}',t-t')\vec{E}(\vec{r}',t')d\vec{r}'\,dt'$$
$$+\int_{-\infty}^{\infty} \chi^{(2)}(\vec{r}-\vec{r}_1,t-t_1;\vec{r}-\vec{r}_2,t-t_2):\vec{E}(\vec{r}_1,t_1)\vec{E}(\vec{r}_2,t_2)d\vec{r}_1dt_1d\vec{r}_2dt_2$$
$$+\int_{-\infty}^{\infty} \chi^{(3)}(\vec{r}-\vec{r}_1,t-t_1;\vec{r}-\vec{r}_2,t-t_2;\vec{r}-\vec{r}_3,t-t_3):\vec{E}(\vec{r}_1,t_1)\vec{E}(\vec{r}_2,t_2)\vec{E}(\vec{r}_3,t_3)d\vec{r}_1dt_1d\vec{r}_2dt_2d\vec{r}_3dt_3$$
$$+\cdots, \qquad (2.10)$$

where the coefficients before the $\vec{E}$s, $\chi^{(1)}(\vec{r}-\vec{r}',t-t)$, $\chi^{(2)}(\vec{r}-\vec{r}_1,\ t-t_1;\vec{r}-\vec{r}_2,t-t_2)$ and $\chi^{(3)}(\vec{r}-\vec{r}_1,t-t_1;\vec{r}-\vec{r}_2,t-t_2;\vec{r}-\vec{r}_3,t-t_3)$ are the linear, second-order, and third-order susceptibilities, respectively, in the time-domain. Within a medium not subject to boundary considerations, $\chi^{(n)}$s as a material property should be same everywhere; that is, $\chi^{(n)}$s are independent of the position vector $\vec{r}$. Although the latter assumption is not always true, for most cases where optical wavelengths are longer than the dimensions of the polarisable units, the spatial dispersion (the $\vec{r}$ dependence) of the susceptibilities, $\chi^{(n)}$, may be justly neglected.

An optical field can be expressed as a group of monochromatic plane waves as

$$\vec{E}(\vec{r},\ t) = \sum_i \vec{E}(\vec{k}_i,\omega_i)$$
$$= \sum_i \mathbf{E}(\vec{k}_i,\omega_i)\,\mathbf{exp}(i\vec{k}_i\cdot\vec{r}_i - i\omega_i t) \qquad (2\text{-}11)$$

with $\vec{k}_i$ being the propagation vector for the i-th monochromatic wave. Substitution of Eq.(2.11) into Eq.(2.10) and use of the Fourier transformation[81]

$$A(t) = \int_{-\infty}^{\infty} A(\omega)\,\mathbf{exp}(-i\omega t)d\omega \qquad (2.12a)$$

with

$$A(\omega) = \frac{1}{2\pi}\int_{-\infty}^{\infty} A(t)\,\mathbf{exp}(i\omega t)dt \qquad (2.12b)$$

gives

$$\vec{P}(\vec{k},\omega) = \vec{P}^{(1)}(\vec{k},\omega) + \vec{P}^{(2)}(\vec{k},\omega) + \vec{P}^{(3)}(\vec{k},\omega)+\cdots \qquad (2.13)$$

with

$$\vec{P}^{(1)}(\vec{k},\omega) = \chi^{(1)}(\vec{k},\omega)\mathbf{E}(\vec{k},\omega) \qquad (2.14)$$

$$\vec{P}^{(2)}(\vec{k},\omega) = \chi^{(2)}(\vec{k}=\vec{k}_i+\vec{k}_j,\omega=\omega_i+\omega_j):\mathbf{E}(\vec{k}_i,\omega_i)\mathbf{E}(\vec{k}_j,\omega_j) \qquad (2.15)$$

and

$$\vec{P}^{(3)}(\vec{k},\omega) = \chi^{(3)}(\vec{k} = \vec{k}_i + \vec{k}_j + \vec{k}_l, \omega = \omega_i + \omega_j + \omega_l) \vdots \mathbf{E}(\vec{k}_i,\omega_i)\mathbf{E}(\vec{k}_j,\omega_j)\mathbf{E}(\vec{k}_l,\omega_l) \tag{2.16}$$

Again we have the relations between polarization, electric field and medium's characteristics similar to Eq. (2.10). But here the $\chi^{(n)}$ s are in the frequency domain. Using the same argument as before, the $\chi^{(n)}$s are $\vec{k}$ independent and are solely functions of the frequencies. The linear polarization $\vec{P}^{(1)}(\vec{k},\omega)$, which has the same frequency ω as the incident optical field, is induced by the field via the linear susceptibility $\chi^{(1)}(\omega)$. The linear dielectric constant $\varepsilon(\omega)$ is related to $\chi^{(1)}(\omega)$ through

$$\varepsilon(\omega) = 1 + 4\pi\chi^{(1)}(\omega). \tag{2.17}$$

For nonlinear processes, the nonlinear polarization may have a frequency differed from the incident ones, and due to the tensor nature of $\chi^{(n)}$, some elements of the $\chi^{(n)}$s may, depending on the process involved, have more dominant effect on the observed total polarization $\vec{P}(\vec{k},\omega)$ than other elements have. It is then necessary to write $\chi^{(n)}$ in the way that the process involved can be identified. The notation convention for $\chi^{(n)}$ is that a negative value of the resultant polarization frequency is put on the first place followed by a semicolon, then come the input optical fields' frequencies with their own sign representing the wave vector direction, so that the total sum of the frequencies in the bracket is zero. For example, for the third-order harmonic generation:

$$\chi^{(3)}(\vec{k} = \vec{k}_i + \vec{k}_j + \vec{k}_l, \omega = \omega_i + \omega_j + \omega_l) \Rightarrow \chi^{(3)}(-3\omega;\omega,\omega,\omega) \tag{2.18}$$

2.2 Basics of the Susceptibilities, $\chi^{(n)}$

As can be seen from Eqs. (2.14)-(2.16), susceptibilities are the quantities that characterize the medium response to the incoming optical fields. The susceptibilities($\chi^{(n)}$s) are in the forms of different rank of tensors. The linear susceptibility $\chi^{(1)}(-\omega;\omega)$ is a second-order tensor having nine elements; the second-order nonlinear susceptibility $\chi^{(2)}(-\omega$

$;\omega_i,\omega_j)$ is a third-order tensor with 27 elements; and the third-order nonlinear susceptibility $\chi^{(3)}(-\omega;\omega_i,\omega_j,\omega_l)$ is a fourth-order tensor with 81 elements. The magnitude and the sign of the elements of $\chi^{(n)}$ are solely determined by the components and the structure of a medium. To identify out materials with large optical nonlinearities, we must first understand the origins of the optical nonlinearities, that is how the elements of the susceptibility tensors are related to the microscopic structure of materials.

To develop expressions for the $\chi^{(n)}$s, we choose a small volume V of the medium. This volume is small enough so that within it the spatial variation of the optical electric field can be ignored, but the volume is sufficiently large so that the number of charged particles (electrons and ion cores) is large enough to wash out the thermal fluctuation of the single particle. To further simplifying the procedure, the interactions between molecules are ignored, which means the density of the molecules is low. In fact, we are going to deal with the single molecule first and sum the individual molecule's effect later to get the $\chi^{(n)}$s for bulk medium.

The procedure used most in deducing expressions for $\chi^{(n)}$s is via the density matrix operator in the energy representation. In this procedure, a density matrix operator ρ is first defined as[34]

$$\rho = \overline{|\psi\rangle\langle\psi|}, \tag{2.19}$$

with

$$\langle\psi|\psi\rangle = 1. \tag{2.20}$$

ψ is the normalized wave function of the medium under the influence of the optical fields, and ρ is the counterpart of the probability in the classic picture.

The electric polarization $\vec{\mathbf{P}}$ has an average value of [34]

$$\begin{aligned}\langle\vec{\mathbf{P}}\rangle &= \langle\psi|\vec{\mathbf{P}}|\psi\rangle \\ &= \mathrm{Tr}(\rho\vec{\mathbf{P}}).\end{aligned} \tag{2.21}$$

In order to obtain $<\vec{P}>$, we need to know the density matrix operator first. The equation of motion for ρ is

$$\frac{\partial \rho}{\partial t} = \frac{1}{i\hbar}[H, \rho] \tag{2.22}$$

with $H = H_0 + H_{int} + H_r$. H_0 is the unperturbed system Hamiltonian, H_{int} is the interaction between medium and the optical electromagnetic fields, and H_r is the thermal disturbance or relaxation term. For a medium where the electronic contribution to the susceptibility is dominant, $H_{int} = e\vec{r} \cdot \vec{E}$. For a medium where the ionic contribution is dominant, $H_{int} = \sum_i (-q_i)\vec{R}_i \cdot \vec{E}$ with q_i and $\vec{R}_i$ being the charge and position of the ith ion.

Substitution of the perturbation expansions

$$\rho = \rho^{(0)} + \rho^{(1)} + \rho^{(2)} + \cdots \tag{2.23}$$

and

$$\begin{aligned} \langle \vec{P} \rangle &= \langle \vec{P}^{(1)} \rangle + \langle \vec{P}^{(2)} \rangle + \langle \vec{P}^{(3)} \rangle + \cdots \\ &= \mathrm{Tr}(\rho^{(1)}\vec{P}) + \mathrm{Tr}(\rho^{(2)}\vec{P}) + \mathrm{Tr}(\rho^{(3)}\vec{P}) + \cdots \end{aligned} \tag{2.24}$$

as well as Eq. (2.11) into Eq. (2.22), and use of the Fourier expansion of the density matrix operator

$$\rho^{(n)} = \sum_i \rho^{(n)}(\omega_i), \tag{2.25}$$

the expressions of $\rho^{(n)}(\omega)$ can be obtained[35]:

$$\rho^{(1)}_{nn'}(\omega_j) = \frac{[H_{int}(\omega_j)]_{nn'}}{\hbar(\omega_j - \omega_{nn'} + i\Gamma_{nn'})}(\rho^{(0)}_{n'n'} - \rho^{(0)}_{nn}) \tag{2.26}$$

$$\rho^{(2)}_{nn'}(\omega_j + \omega_k) = \frac{[H_{int}(\omega_j), \rho^{(1)}(\omega_k)]_{nn'} + [H_{int}(\omega_k), \rho^{(1)}(\omega_j)]_{nn'}}{\hbar(\omega_j + \omega_k - \omega_{nn'} + i\Gamma_{nn'})}. \tag{2.27}$$

With the substitution of $H_{int} = e\vec{r} \cdot \vec{E}$ and $\vec{P} = -Ne\vec{r}$ into Eqs. (2.26) and (2.27), the macroscopic susceptibilities can be obtained from Eq. (2.24). The expressions for the linear, second-order and third-order $\chi^{(n)}$ are presented:

$$\chi_{ij}^{(1)}(-\omega,\omega) = \frac{P_i^{(1)}(\omega)}{E_j(\omega)}$$

$$= N\frac{e^2}{\hbar}\sum_{a,b}\left[\frac{(r_i)_{ab}(r_j)_{ba}}{\omega+\omega_{ba}+i\Gamma_{ab}} - \frac{(r_j)_{ab}(r_i)_{ba}}{\omega-\omega_{ba}+i\Gamma_{ba}}\right]\rho_g^{(0)}, \tag{2.28}$$

$$\chi_{ijk}^{(2)}(-\omega;\omega_1,\omega_2) = \frac{Ne^3}{\varepsilon_0 2\hbar}S_0\sum_{a,b,c}\left[\frac{(r_i)_{ab}(r_j)_{bc}(r_k)_{ca}}{(\omega_{ba}-\omega_1-\omega_2)(\omega_{ca}-\omega_2)}\right.$$
$$+\frac{(r_j)_{ab}(r_i)_{bc}(r_k)_{ca}}{(\omega_{ba}+\omega_1)(\omega_{ca}-\omega_2)}$$
$$\left.+\frac{(r_i)_{ab}(r_j)_{bc}(r_k)_{ca}}{(\omega_{ba}+\omega_1)(\omega_{ca}+\omega_1+\omega_2)}\right]\rho_g^{(0)}, \tag{2.29}$$

and

$$\chi_{ijkl}^{(3)}(-\omega;\omega_1,\omega_2,\omega_3) = \frac{Ne^4}{\varepsilon_0 3!\hbar^3}S_0\sum_{a,b,c,d}\left[\frac{(r_i)_{ab}(r_j)_{bc}(r_k)_{cd}(r_l)_{da}}{(\omega_{ab}-\omega_1-\omega_2-\omega_3)(\omega_{ca}-\omega_2-\omega_3)(\omega_{cd}-\omega_3)}\right.$$
$$+\frac{(r_j)_{ab}(r_i)_{bc}(r_k)_{cd}(r_l)_{da}}{(\omega_{ba}+\omega_1)(\omega_{ca}-\omega_2-\omega_3)(\omega_{da}-\omega_3)}$$
$$+\frac{(r_j)_{ab}(r_k)_{bc}(r_i)_{cd}(r_l)_{da}}{(\omega_{ba}+\omega_1)(\omega_{ca}+\omega_2+\omega_3)(\omega_{da}-\omega_3)}$$
$$\left.+\frac{(r_j)_{ab}(r_k)_{bc}(r_l)_{cd}(r_i)_{da}}{(\omega_{ba}+\omega_1)(\omega_{ca}+\omega_1+\omega_2)(\omega_{da}+\omega_1+\omega_2+\omega_3)}\right]\rho_g^{(0)} \tag{2.30}$$

In the equations above, ω is the frequency of the response of the medium; ω_1,ω_2 and ω_3 are the frequencies for the incoming optical fields; $\rho_g^{(0)}$ is the density matrix operator for the system at the ground state at thermal equilibrium and is given by the Boltzmann distribution for a molecular medium; ω_{xy} is a molecular transition frequency which relates the system energy levels E_x and E_y by $\hbar\omega_{xy} = E_x - E_y$; $(er_i)_{ab} = \langle a|er_i|b\rangle$ represents the dipole moment of state $|a\rangle$ when a = b and corresponds to a transition dipole moment between two states $|a\rangle$ and $|b\rangle$ when $a \neq b$; and S_0 is the symmetrizing operation which describes the intrinsic symmetric properties of the $\chi^{(n)}$ regardless the type of the medium. As a reminder, the damping effect, Γ, is not considered in the $\chi^{(2)}$ and $\chi^{(3)}$ expressions to make the formula more compact. Of course this is valid only for the case of no or little absorption.

The complete set of the second-order susceptibility $\chi^{(2)}$ has 27 elements while the third-order susceptibility $\chi^{(3)}$ has 81 elements[36]. According to the type of the point symmetry of the structure, not all of the elements are independent. A symmetric operator S is defined as an operation under which the medium is spatially invariant. Therefore, $\chi^{(n)}$ shall remain unchanged under a symmetric operation. S itself is a second-rank three-dimensional tensor. For the second-order susceptibility $\chi^{(2)}$, the symmetry operation is:

$$(\hat{i} \cdot S^{+}) \cdot \chi^{(2)} : (S \cdot \hat{j})(S \cdot \hat{k}) = \chi^{(2)}_{ijk}. \tag{2.31}$$

An immediate result of the above relationship is that for a medium with inversion symmetry, its second-order susceptibility is equal to zero, which can be seen as follows. Since for inversion symmetry

$$S \cdot \hat{e} = -\hat{e}, \tag{2.32}$$

the substitution of Eq.(2.32) into Eq.(2.31) gives

$$\chi^{(2)}_{ijk} = -\chi^{(2)}_{ijk}. \tag{2.33}$$

The only solution of Eq.(2.33) is that

$$\chi^{(2)}_{ijk} = 0. \tag{2.34}$$

Hence, in a medium of isotropic or cubic symmetry, the third-order nonlinearity is the lowest observable nonlinear optical phenomenon. As a matter of fact, $\chi^{(n)}$ vanishes for all n of the even numbers in a medium of inversion symmetry. However, it needs to be pointed out that the conclusions above are only true when all multipoles higher than the electric dipole are ignored.

The type of point group symmetry that a medium possesses also determines the number of independent elements in a susceptibility tensor. Here we simply list the relationship between elements of the $\chi^{(3)}$ tensor for commonly encountered crystal class of medium in Table 2.1.[37]

TABLE 2.1 Independent Nonvanishing Elements of $\chi^{(3)}$ Tensor for Crystals of Certain Symmetry Classes

Symmetry Class	Independent Nonvanishing Elements
Triclinic	All 81 elements are independent and nonzero
Tetragonal	xxxx = yyyy, zzzz
422, 4mm	yyzz = zzyy, zzxx = xxzz, xxyy = yyxx, yzyz = zyzy,
4/mmm, $\bar{4}$2m	zxzx = xzxz, xyxy = yxyx, yzzy = zyyz, zxxz = xzzx xyyx = yxxy
Cubic	xxxx = yyyy = zzzz, yyzz = zzxx = xxyy,
23, m3	zzyy = yyxx = zzxx, zyzy = xzxz = yxyx, yzyz = zxzx = xyxy, zyyz = xzzx = yxxy, yzzy = zxxz = xyyx
432, $\bar{4}$3m, m3m	xxxx = yyyy = zzzz yyzz = zzyy = zzxx = xxzz = xxyy = yyxx yzyz = zyzy = zxzx = xzxz = yxyx = xyxy yzzy = zyyz = zxxz = xzzx = xyyx = yxxy
Hexagonal	zzz, xxxx = yyyy = xxyy + xyyx +xyxy
622, 6mm	xxyy = yyxx, xyyx = yxxy,xyxy = yxyx
6/mmm, $\bar{6}$m2	yyzz = xxzz, zzyy = zzxx, zyyz = zxxz yzzy = xzzx, yzyz = xzxz, zyzy = zxzx
Isotropic	xxxx = yyyy = zzzz yyzz = zzyy = zzxx = xxzz = xxyy = yyxx yzzy = zyyz = zxxz = xzzx = xyyz = yxxy xxxx = xxyy + xyxy + xyyx

From the expression for $\chi^{(3)}$, Eq.(2.30), if all integrations $(r_i)_{ab}$ and the transition frequencies ω_{ab} are known, there is no difficulty in calculating every element for the third-order susceptibility $\chi^{(3)}$ tensor. It is not possible, however, to obtain the exact wave functions and the eigenvalues at all different energy levels. One possible computational approach to the calculation of the nonlinear susceptibility is to assume a situation where the frequencies of the incoming optical fields, as well as their combinations, are far from the resonance. Thus we can replace each frequency denominator in the $\chi^{(3)}_{ijkl}$ by an average value and bring all frequency denominators out of the summations. The problem is then reduced to finding the ground-state eigenfunction of the system, and using the eigenfunction's closure properties to get the element $\chi^{(3)}_{ijkl}$ through the moments of the ground-state charge distribution[38]. Nevertheless, this procedure can hardly provide a satisfactory result for the nonlinearities.

Due to the complexity of organic compounds, various approximations have been suggested. Instead of using the ab initio method that accounts for the contribution from all σ and π electrons, some methods neglect the effects of the σ electrons (PPP Method)[39,40]. Other methods only consider the contribution from the valence electrons and neglect the overlap between the atomic orbitals to various degrees, such as the Complete Neglect of Differential Overlap Method,[75] Intermediate Neglect Differential Overlap Method,[76] Modified Neglect of Diatomic Overlap Method,[77] and so forth. The object of all these approximations is to make the calculation of the third-order susceptibility $\chi^{(3)}$ possible for the organic materials.

To minimize the error caused by these approximations and to simplify further the calculation procedure, some experimental data can be used. The principle of the self-consistent theorem is introduced. That is, if a set of eigenfunctions of the organic system, calculated through the use of some experimental data, describes the state of the system well, the properties of the system obtained from the eigenfunctions should be in agreement with the corresponding experimental data. The parameters of the formulas are modified

continually to allow the best fit of the results. However, even for these semi-empirical methods, only the comparison data of the third-order susceptibility $\chi^{(3)}$ can be obtained at the present time, especially when the delocalization of the π-electron is over the entire molecular structure.[41]

2.3 Degenerate Four-Wave Mixing

Let us return to the wave equation, Eq. (2-7),

$$\nabla^2\vec{E} - \left(\frac{n_0}{c}\right)^2 \frac{\partial^2\vec{E}}{\partial t^2} = \frac{4\pi}{c^2}\frac{\partial^2\vec{P}}{\partial t^2}. \tag{2.35}$$

Since we are most interested in the nonlinear response, the polarization $\vec{P}$ is rewritten as

$$\vec{P} = \vec{P}^{L} + \vec{P}^{NL}. \tag{2.36}$$

Again, we use Eq.(2-11) in the time domain

$$\vec{E}(\vec{r},t) = \sum_i \mathbf{E}(\vec{r},t)\exp\left[-i\left(\omega_i t - \vec{k}\cdot\vec{r}\right)\right] + c.c. \tag{2.37}$$

This time, $\vec{E}(\vec{r},t)$ is represented in the time domain and c.c. is the complex conjugate. In writing $\vec{E}(\vec{r},t)$ in this form, we have assumed that the optical field can be expressed as a group of monochromatic plane waves and each of the monochromatic waves is a product of one component oscillating at the optical frequency of the laser and another component $\mathbf{E}(\vec{r},t)$ which changes at a much slower frequency. The latter assumption is called the slowly-varying-envelope approximation (SVEA). The SVEA is widely used to make the wave analysis simple and is well satisfied for most laser sources. For example, the laser sources used in the experiments usually have a pulse width ranging from 20 nS to 10 pS (20×10^{-9} - 10×10^{-12} second), and a green light (λ = 532 nm) out from a KDP doubler of a Nd:YAG laser has a period of merely 1.8×10^{-16} second. Thus the change of the optical field amplitude along the propagation is very slow when compared to the optical frequency.

The most significant result of the SVEA is the relationship

$$\left|\frac{\partial^2}{\partial z^2}\mathbf{E}(z)\right| << \left|k\frac{\partial}{\partial z}\mathbf{E}(z)\right| << \left|k^2\mathbf{E}(z)\right|, \tag{2.38}$$

with $\mathbf{E}(\vec{r}, t)$ being the slowly varying amplitude of the optical field. This relation is used to eliminate the coupling of the differential wave components in solving for the polarization $\vec{P}$.

Similarly, the nonlinear polarization can be expressed as

$$\vec{P}^{NL} = \sum_i \mathbf{P}(\vec{r}, t) \exp\left[-i\left(\omega_i t - \vec{k}_i \cdot \vec{r}\right)\right] + c.c. \tag{2.39}$$

Again, $\mathbf{P}(\vec{r}, t)$ here represents the slowly varying amplitude of the nonlinear response and has the vector characteristics of the $\vec{P}^{NL}$.

For the sake of simplicity, only the situation where the medium is of the isotropic or cubic group symmetry will be considered. The lowest order of the nonlinear phenomenon is due to $\vec{P}^{(3)}$, and we neglect the higher orders of the nonlinear polarizations.[34] Furthermore, we consider the case of degenerate four-wave mixing where all four waves involved have the same frequency and the two pump waves are usually of the same intensity. Near the frequency ω, the medium is assumed to be transparent and nondispersive to the incoming waves. The temporal parts are also dropped, which means the results are for the steady state only. The basic geometry of DFWM is shown in Figure 2.1.

Substitution of Eqs. (2.37) and (2.39) into Eq. (2.35), and with the use of the SVEA relation (2.38), give the wave equation for the ith polarization component of the conjugate wave $E_{c,i}$:[11]

$$\frac{dE_{c,i}}{dz} = i\frac{2\pi}{n_0} P_i \exp\left[-i\left(-\vec{k}_c + \vec{k}_b + \vec{k}_f + \vec{k}_p\right) \cdot \vec{r}\right] \tag{2.40}$$

The term $-\vec{k}_c + \vec{k}_f + \vec{k}_b + \vec{k}_p = \Delta\vec{k}$ is called the phase mismatch of the process, which describes the relative phase difference for all four wave vectors. For a cumulative build up of the reflected field E_c, the phase mismatch $\Delta\vec{k}$ must be equal to or near zero. In the case of $\Delta\vec{k}$ being zero, the phase match is said to be achieved and E_c has the maximum

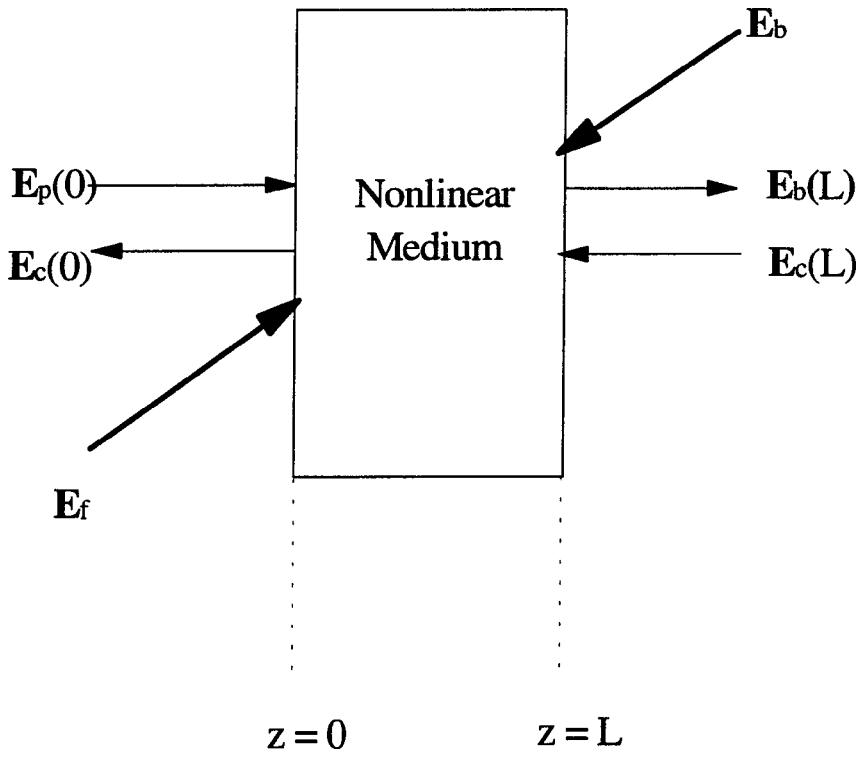

Figure 2.1 The basic geometry of phase conjugation by the backward DFWM. The counter-traveling pump waves $\mathbf{E}_f$ (forward) and $\mathbf{E}_b$ (backward) are assumed to be nondepleted. $\mathbf{E}_p$ is the probe wave of much weaker intensity and $\mathbf{E}_c$ is the conjugate wave. All four waves have the same optical frequency

amplitude. If the two pump waves are traveling in exactly counter directions, that is, $\vec{k}_f + \vec{k}_b = 0$, then there must be

$$\vec{k}_c = -\vec{k}_p, \tag{2.41}$$

which means the reflected wave will retrace the probe wave with the reversed space phase factor of the original beam. This is the reason the reflected wave is usually referred to as the conjugate reflection of the probe beam. The explanation of the phase match from the point of view of quantum theory is that the total momentum of the photon involved in the process should be conserved and the momentum is defined as $\vec{p} = \hbar\vec{k}$.

The phase match in the four-wave mixing process is a strict condition. For example, in case of the third-order harmonic generation (THG), which is a special case of the four-wave mixing with the three input waves being collinear, the phase match demands that $n(\omega) = n(3\omega)$ to have high conversion efficiency.[35]

The solutions of Eq.(2.40) are obtained through the procedure of combining Eq.(2.37) and (2.39), and assuming that pump beams are much more intensive than both the probe and the conjugate beams,[11]

$$\mathbf{E}_c(0) = -i\left[\left(\frac{\kappa^*}{|\kappa|}\right)\tan(|\kappa|L)\right]\mathbf{E}_p^*(0), \tag{2.42}$$

with the parameter κ^* defined as

$$\kappa^* = \frac{2\pi\omega}{cn_0}\chi^{(3)}E_f E_b. \tag{2.43}$$

Here, $\mathbf{E}_c(0)$ represents the conjugate field strength at the reflection surface of the sample, and L is the thickness of the sample. Note that in the deduction of the above solution, pump power depletion is ignored.

Again we see that the reflected field $\mathbf{E}_0$ is the product of a constant (determined by the experimental parameters) and a conjugate replica of the input probe field $\mathbf{E}_p$. In the

practical situation, it is the conjugate beam intensity that is measured. We rewrite Eq. (2.42) in the intensity form:

$$I_c = \tan^2(\kappa L)\cdot I_p \tag{2.44}$$

In most cases, the conjugate signal is much weaker than the probe beam, i.e. $\kappa L < 1$ due to the difficulty of the beam alignment. The reflectivity $R = \tan^2(\kappa L)$ can then be expanded as a power series expansion and only the first term is retained.

$$I_c \approx (\kappa L)^2 I_p, \tag{2.45a}$$

or

$$I_c = \left[\frac{2\pi\omega}{cn_0}\chi^{(3)}(-\omega;\omega,-\omega,\omega)E_fE_b\right]^2\cdot I_p. \tag{2.45b}$$

Since $I = \frac{cn_0}{8\pi}E_f^{\,2} = \frac{cn_0}{8\pi}E_b^{\,2}$ (based on the assumption of the same intensity for the forward and the backward beams), Eq. (2.45b) changes to

$$\begin{aligned} I_c &= \left\{\left(\frac{2\pi\omega L}{c}\right)^2\left(\frac{8\pi}{cn_0}\right)^2\frac{\left[\chi^{(3)}(-\omega;\omega,-\omega,\omega)\right]^2}{n_0^{\,2}}\right\}\cdot I^2\cdot I_p \\ &= \left\{A\,\frac{256\pi^4\omega^2}{c^3}\cdot L^2\cdot\frac{\left[\chi^{(3)}(-\omega;\omega,-\omega,\omega\right]^2}{n_0^4}\right\}\cdot I_0^3 \end{aligned} \tag{2.45c}$$

In Eq. (2.45c), A is a constant determined by how I_f, I_b, and I_p are derived from the same laser source; I_0 is the laser intensity. For example, if I_p is 10% of the main beam, and I_f and I_b are of equal intensity, $A = \frac{10}{100}\cdot\frac{90/100}{2}\cdot\frac{90/100}{2} = 0.02025$. Because we usually use the laser beams in a linearly polarized state, the scalar forms are used instead of the vector form here.

In the deduction of the reflectivity Eq. (2.45c), a transparent medium is assumed, which enables us to drop the damping term. In reality, absorption brings many effects into the third-order susceptibility $\chi^{(3)}(-\omega;\omega,-\omega,\omega)$ for the degenerate four-wave mixing process, usually leading to the increase of the $\chi^{(3)}(-\omega;\omega,-\omega,\omega)$ value and enlarging the relaxation

time when considering the temporal domain changes. If the laser wavelength is far away from the resonance, we can consider only the absorption effect that weakens the intensity of the forward, backward, and probe beams. The correction to Eq. (2.45c) is relatively easy to make and will be described in the next chapter.

CHAPTER 3

EXPERIMENTAL WORK IN DFWM

3.1 Forward-type DFWM Experiment Apparatus

Degenerate four-wave mixing (DFWM) is a nonlinear process involving four interacting optical waves of the same frequency. Unlike the SHG, DFWM is allowed in all types of materials. Although there are many types of configurations for DFWM, they can generally be grouped into two types, the forward method and the backward method. The principle arrangements for these two methods are shown in Figure 3.1.

In the forward configuration, two pump beams $\mathbf{E}_1$ and $\mathbf{E}_2$ are collinear. They could be one intense beam, which means the beams are of same polarization; or they could be distinguished by the different polarization directions. The disadvantages of this configuration are that the phase match constraint limits the angular spread of the probe wave to $\theta \leq (\lambda/l)^{1/2}$ with l being the interaction length and the limited spatial bandwidth of the conjugate beam causes signal distortions.[42] Because of the near collinear propagating of pump and probe waves, either the angular or polarization separation techniques should be utilized to distinguish the conjugate signal from the input fields. These disadvantages of the forward method shadow its easy beam alignment in setup and limit the practical application of the phenomenon.

The backward method does not have the limitations mentioned for the forward method and very much resembles the actual configuration of the applications. The principle of backward DFWM has been shown in Figure 2.1.

In Figure 2.1, $\mathbf{E}_f(\vec{\mathbf{k}}_f, \omega)$ and $\mathbf{E}_b(\vec{\mathbf{k}}_b, \omega)$ are two exactly counter propagating pump waves, and are called the forward and backward pump waves, respectively.

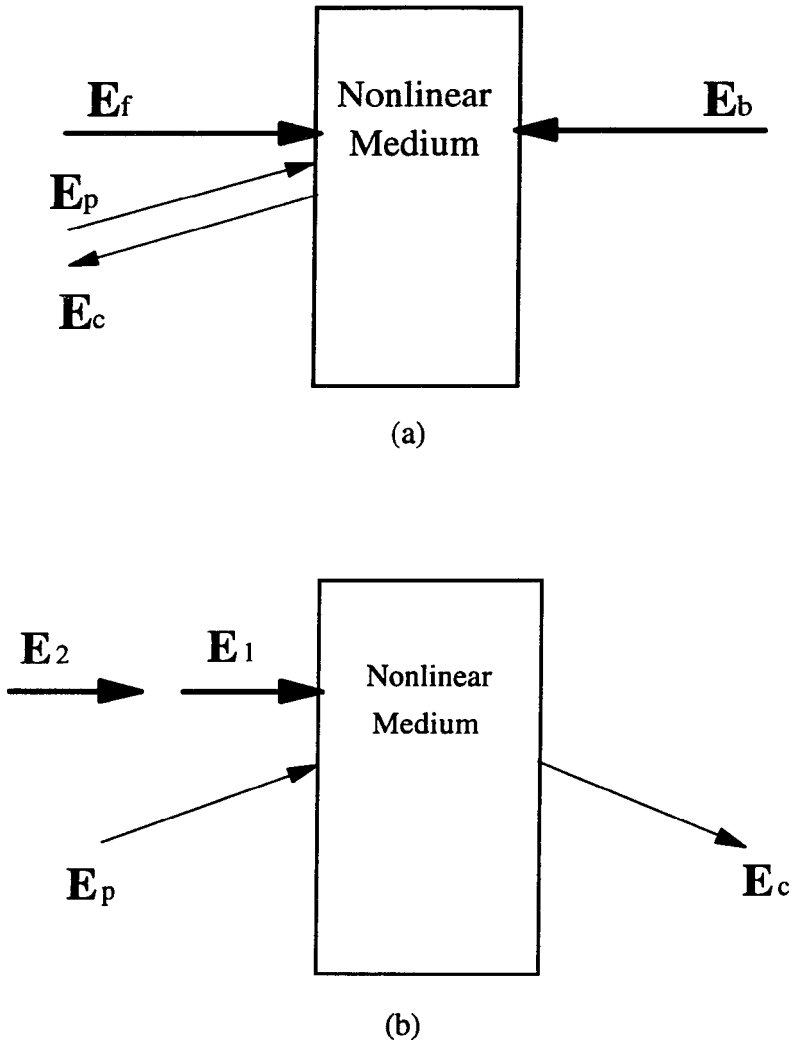

Figure 3.1 Two different types of setup for degenerate four-wave mixing. (a) The backward-type, where two pump beams are counter-traveling. (b) The forward-type where two pump beams are collinear but have different polarizations

$\vec{E}_p(\vec{k}_p, \omega)$ is the probe beam with the same frequency as the pump beam but with much weaker intensity. Usually these beams are derived from the same laser source. The probe beam makes some angle with the forward beam. As discussed in Chapter 2, to get an enhanced conjugate signal output, the phase matching condition must be satisfied, that is, directions for the conjugate beams in both (a) and (b) are determined by the phase match condition

$$\Delta\vec{k} = \vec{k}_f + \vec{k}_b + \vec{k}_p + \vec{k}_c = 0. \tag{3.1}$$

Since $\mathbf{E}_f(\vec{k}_f, \omega)$ and $\mathbf{E}_b(\vec{k}_b, \omega)$ are exactly counter propagating, $\vec{k}_f + \vec{k}_b = 0$. Then Eq. (3-1) changes to

$$\vec{k}_c = -\vec{k}_p \tag{3.2}$$

Thus the phase match requires that the conjugate signal wave $\mathbf{E}_c(\vec{k}_c, \omega)$ propagate in the direction that retraces the probe wave.

As long as the intensities of the two pump waves are the same (see Chapter 2), there is no limitation on the angle θ, though the conjugate signal intensity does change when the angle θ changes. This dependence of the conjugate signal intensity on the angle θ can be easily understood from Eq. (2-44c), which shows $I_c \propto L^2$. The interaction length L is the measure of the overlap of the probe beam with the pump beams. When the beams' cross-section profiles stay the same, the smaller the angle θ is, the longer the beam overlap region will be. In the extreme case where the probe beam is collinear with the forward pump beam, we have the longest interaction length L. However, said collinear beam configuration makes separating the conjugate signal, which retraces the probe beam, from the intense backward pump beam difficult. Thus in most DFWM reported so far, the angle θ is set to a small value ($0 < \theta << 1$ radians) in a compromise of getting as large a conjugate signal as possible while at the same time avoiding the problem of separating the signal from the backward pump beam.

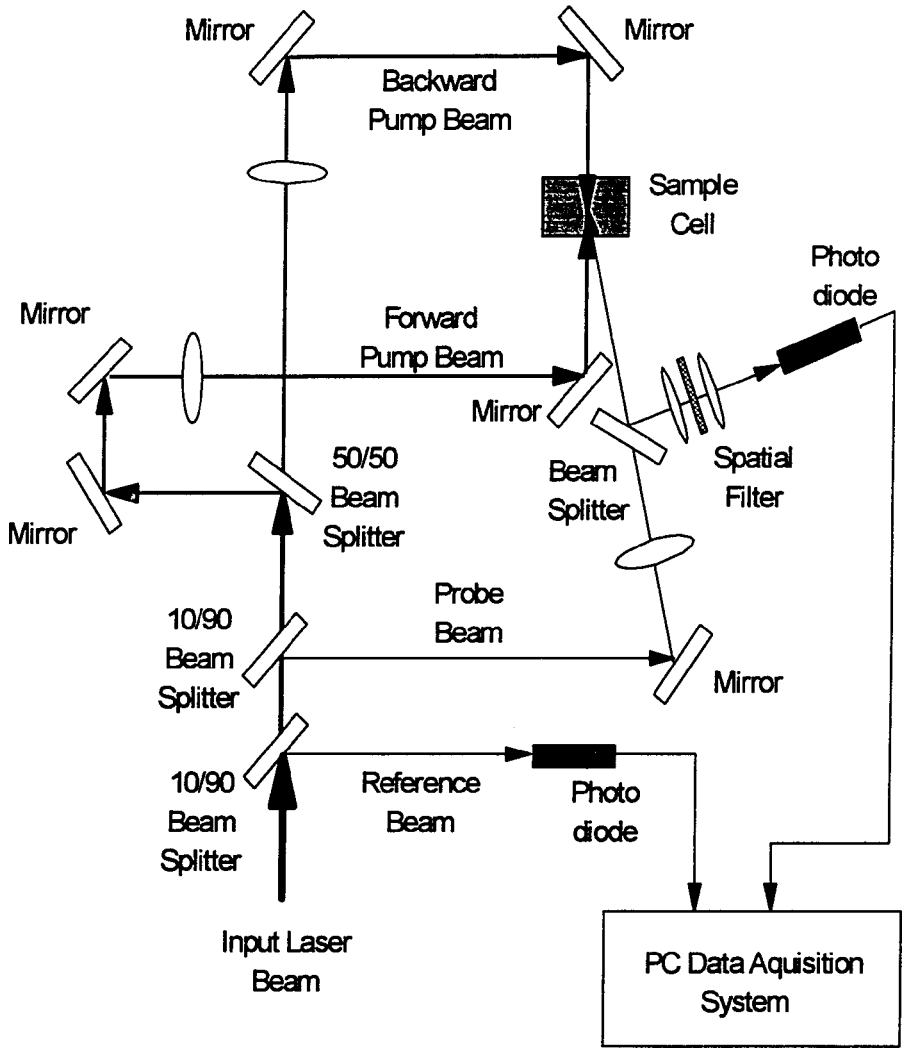

Figure 3.2 The layout of DFWM in the backward-type configuration. The laser source is a Pockers'-cell Q-switched Nd:YAG laser working at 2 pps. The wavelength of the laser beam after passing through a KDP frequency doubler is 532 nm

We choose the backward-type DFWM configuration. The actual layout of the experiment is shown in Figure 3.2.

The light source of our experiment is a pulsed Nd:YAG laser with a Pockels-cell Q-switch. The output beam of the laser has a wavelength of 1064 nm. The maximum output energy for the laser is around 7 mJ when the laser is operated at a rate of 2 pps (pulse-per-second). A KDP frequency doubler is employed to change the laser output frequency from infrared to green light of a wavelength of 532 nm. KDP (potassium dihydrogen phosphate) is of the crystal class $\bar{4}2m$ in the tetragonal system with a large second-order optical nonlinearity $\chi^{(3)}$. Its efficiency in second-harmonic generation is around 20%. Thus, the green light in our experiment has a maximum output energy of 1.4 mJ .

Since an absolute measurement of $\chi^{(3)}$ is very difficult and involves strict system calibration each time in making a measurement, we adopted the comparison measurement method. In this method, the true optical nonlinearity for a sample is obtained from the comparison of the experimental data to that of a standard reference sample of a known nonlinearity.

The laser light has a power variation of $\pm 5\%$. To monitor and eliminate the error in the experimental data due to the laser power fluctuations, the laser beam first goes through a glass plate. The reflection from the glass enters a photo-diode, called the reference signal detector. The output of the reference detector is proportional to the input laser power for each shot. The beam then passes through a beam splitter in a ratio of 10/90. A beam with 10% of the incoming beam intensity is reflected towards a mirror. This reflected beam is employed as the probe beam. The remaining 90% of the incoming beam goes further through another beam splitter in the ratio of 50/50, which means half of the beam passes through and half of the beam is reflected from the splitter. The beam passing through the splitter acts as the backward pump beam, while the reflected beam acts as the forward pump beam after it passes through a translation delay stage.

The angle between the probe beam and the forward beam is about 9° or 0.15 radian. The optical path for each of the three beams is around 76 cm with an error range of 0.5 cm. Our laser has a pulse duration (half width) of 20 ns, which is measured by a Tektronix digital oscilloscope, model 2430A. The coherence length for a continuous wave (CW) can be obtained through the following formulas:[43]

$$\Delta\lambda \cong \frac{\lambda_0^2}{c\Delta t}, \tag{3.3a}$$

and

$$\Delta x = \frac{\lambda_0^2}{\Delta\lambda}. \tag{3.3b}$$

Here, $\Delta\lambda$ represents the wavelength spread, λ_0 is the characteristic wavelength, and Δt is the duration of the spikes within the laser pulse. The typical coherence length, Δx, for a Q-switched pulsed Nd:YAG laser is in the range of cm.[78] So, for the laser light duration of the nm range, the demand for the three beams' path lengths being within the coherence length is not difficult to satisfy. For pico-second duration pulses, the coherence length reduces to sub-mm, and the beam path length adjustment is much more difficult to satisfy.

Because all three beams here are derived from a single beam source that has an electric field polarization perpendicular to the direction of the wave propagation vector, all input beam electric fields are parallel and in the y-axis direction.

The two pump beams are weakly focused at the sample cell so that there is enough power density in the sample region to observe the third-order nonlinear optical phenomenon without damaging the sample cell and vaporizing the sample solution. The weakly focused beams also make the interaction length longer and the beam alignment much easier. The two pump beams have a diameter of about 0.1 mm, and the power density for the pump beams in the sample region is around 0.11 GW/cm^2.

The sample handling system is illustrated in Figure 3.3. The sample solution reservoir is a 5-ml medical syringe with a rubber cork on the opening. The pump is a model RP-G20 made by Fluid Metering, Inc. The filter, a PTFE syringe filter, is a "use-

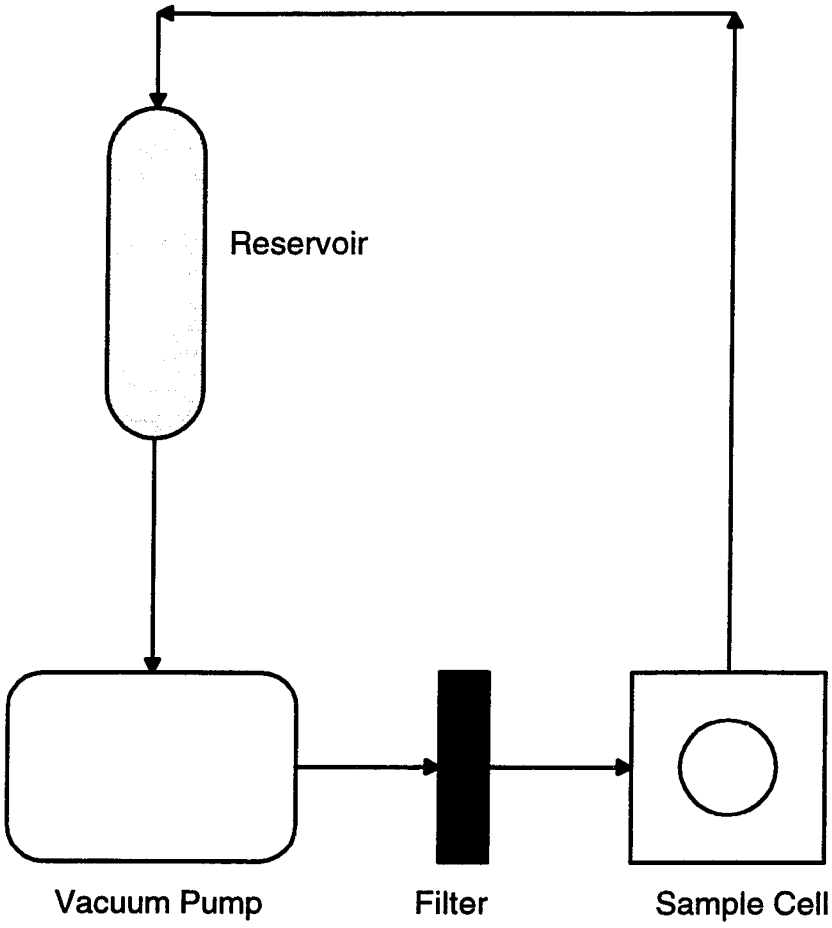

Figure 3.3 Sample solution closed loop filtration system. The sample cell has a depth of 10 mm. The whole sample handling system is isolated from the environment

then throw" type made by Acrodisc with a pore size of 0.2 micro-meter. The sample cell consists of three pieces of Aluminum block with a hole of 10-mm diameter in the middle. Two pieces of microscope glass slides are bolted between the aluminum blocks. The gasket is made of Teflon. The sample cell has a depth of 10 mm. There are two small holes on the top and the side-bottom on the sample cell for sample solution passage in and out of the cell. The sample cell is mounted on an eight-way adjustable stage. The adjustment of the sample position and orientation can be easily achieved. The whole sample system is connected by Teflon tubing and is insulated from the environment. These measures ensure the minimum contamination to the sample solution.

The sample solution pump has a capacity of 6 ml per minute and is run only when not taking data to avoid the influence of vibration. For air-sensitive samples, nitrogen gas can be charged into the sample solution reservoir to propel air out of the sample system.

The conjugate signal is maximum when the two pump beams are set exactly in counter-propagating and the probe beam passes through the overlap region. The conjugate signal beam retraces the probe beam and, after reflected at a mirror, is focused to fit the pinhole opening of a spatial filter. The spatial filter, functioning by the principle of Fourier transformation, blocks out most of the detectable optical background noise. Out from the spatial filter, the conjugate signal is then picked up by a photo-diode detector. The converted electric signal is then sent to the data acquisition system that is shown as Figure 3.4.

As seen in Figure 3.4, the conjugate optical beam shines on a photo-diode. The generated electric pulse goes through an amplifier. The peak-detector picks up the signal's peak value and sends the captured peak value to a PC based data acquisition system. The reference signal, after being amplified, is divided into two channels. One of the two channels is stretched and delayed for 15 μs. The stretched and delayed signal then acts as a trigger signal to trigger the PC base data acquisition system. The reason for using the reference signal as the trigger signal is because of the relatively stable intensity of the

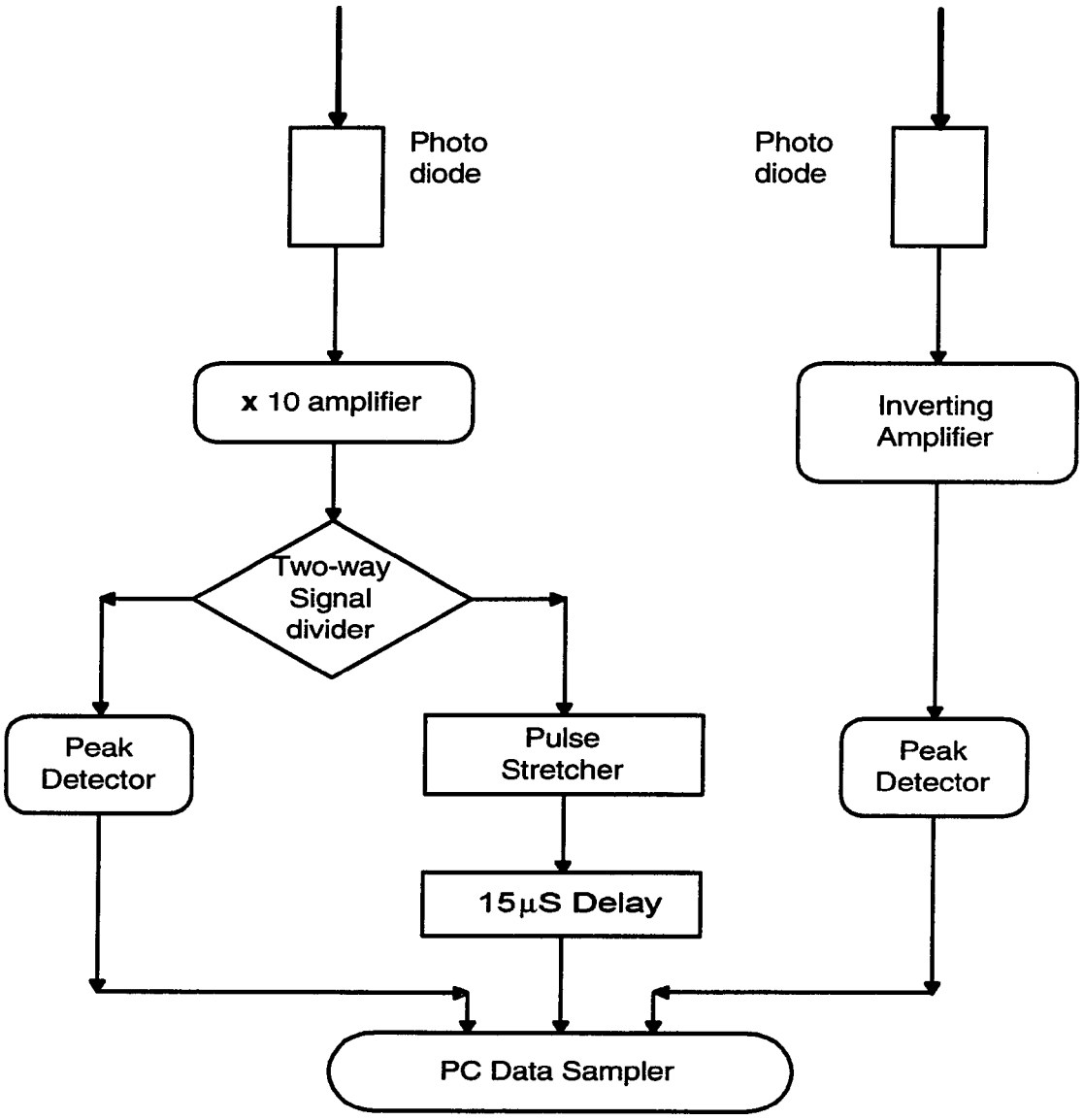

Figure 3.4 Schematic of the data acquisition system. Two peak detectors grab the intensity of both reference and conjugate signals. The trigger signal is supplied by the reference because of its strength being at a constant level. Both reference and conjugate are sent to a PC based sampler that also acts as an analog to digital transformation

reference beam (about 5% variation as mentioned before). Another pulse from the reference enters a peak-detector, and the peak value that is proportional to the laser intensity is sent to the PC data acquisition system.

The PC data acquisition system consists of an IBM-compatible 286 personal computer, a high-speed data sampler of the model DT-2821F-SE made by Data Translation, Inc., and accompanying control software. The high-speed sampler also acts as an analog to digital conversion device.

The PC data acquisition system controls the gain of the incoming signal and the number of samples per cycle (500 data per point is used in our experiment), and calculates the mean and the standard deviation for the conjugate and the reference signal respectively. It then stores the data in a disk data file. A separate FORTRAN program is employed to calculate the ratio of the conjugate to the cube of the reference, Sig./Ref^3. This enables us to minimize the error caused by the laser power fluctuation as can be seen from Eq. (2-45c). This program goes further to purge those data with an error larger than three times of the standard deviation. It then recalculates the mean and standard deviation and checks the data again until all data are within the range of the three times of the standard deviation. In our observation, in the 500 data collected, 3 to 50 are out of the 3σ region for each group.

3.2 Sample Preparation

The samples are synthesized and characterized by a group lead by Gray et al.[44] As time passes, some complexes might have decomposed. The decomposition is evidenced by changing sample solution color from clear colorless to light brown or yellowish.

The first step in preparing samples is to recrystallize them. There is a standard procedure that involves dissolving the sample (in crystal state) in methylene chloride (CH_2Cl_2), filtering the solution through a layer of the silicon gel, adding Hexane, which has a higher vaporizing temperature and is a poor solvent for the samples, to the solution, then heating the mixture at a temperature between the vaporizing points of CH_2Cl_2 and of

Hexane. As the CH_2Cl_2 being vaporized, the solubility of the mixture becomes lower. When the tiny crystals can be seen to condense out, the heater is turned off and the solution is placed into a refrigerator. The low temperature further decreases the solubility, and clean crystals can finally be obtained.

The sample in the DFWM is in the liquid state. The liquid sample has the advantages of fast self-healing from the possible laser damage, precise control of the concentration, and easy handling. However, in most potential applications, the nonlinear materials are usually in the thin-film or single-crystal form. Some strong electric field poling techniques have been utilized to align the molecules to enhance the nonlinear optical phenomenon. Even though the liquid sample is not in the form of its application, the information about the single molecule's nonlinear optical property can still be obtained from the bulk materials' nonlinear optical response. The fact that second-order nonlinear effect diminishes in the isotropic liquid further simplifies the job in analyzing the experimental result.

The solvent is tetrahydrofuran (THF), which has a good solubility for most of our samples and offers the advantage of wide optical transparency throughout the visible light range. The low third-order optical nonlinearity of THF ensures a minimum contribution from the solvent to the measured second-order molecular hyperpolarizability. In the case where THF cannot dissolve the sample, CH_2Cl_2 is used.

The sample solution is injected into the sample reservoir. We usually run the pump for 4 minutes before taking data to filter out the dust and to mix the solution well. Changing the concentration is accomplished by adding high concentration sample solution to the reservoir and by running the pump to mix the high concentration solution with those already in the system. Once proper sample concentration is reached, measures of shielding light out off the reservoir are taken. Most of our samples are sensitive to UV light and will change color from clear colorless to dark black in about 20 hours if exposed to light. When shielded from UV light, the samples can stay in a clear colorless state for several

days. For most samples, we measure the $\chi^{(3)}$ value at a concentration from 10^{-2} to 10^{-4} molarity (mole per liter).

3.3 Measurements and Evaluation of Molecule Hyperpolarizability, $\gamma^{(2)}$

First, we measure the third-order conjugate signal of carbon disulphide(CS_2) which has been widely used as the standard reference material. Careful optical path adjustments for all three beams (two pumps and one probe) are done at this stage to optimize the optical system. The achievement of the optimized optical system is evidenced from the strongest conjugate signal output. The whole optical system must not be touched once the strongest conjugate signal is detected. The conjugate signal intensity for CS_2 is recorded as the reference for the following comparative measurements.

Second, the sample system is rinsed with THF (with CH_2Cl_2 in the case of using CH_2Cl_2 as solvent) three times, and the conjugate signal for the solvent is measured. Some high concentration sample solution is then added to the sample system until the desired concentration is achieved. Then the conjugate signal is measured. The procedure is repeated for all desired concentrations. Usually, seven to ten groups of data are taken. As noted before, each group contains 500 repeated conjugate signal readings.

Finally, the sample system is rinsed with CS_2 and the conjugate signal for CS_2 is taken again. The two measurements of CS_2 are used to make sure that the optical configuration is the same for all data.

As mentioned before, a comparison technique is used. This avoids the trouble in getting details about the optical system, which includes beam interaction length, the angle between probe beam and the forward pump beam, and the wave intensities for all three input beams, as well as the degenerate factors in Eq.(2.44c). In using the comparison technique, $\chi^{(3)}$ values (which are proportional to the conjugate signal intensity) of the sample solutions at different concentrations are obtained by comparing the values of the conjugate signal to that of the pure CS_2 solution.

In deducing Eq. (2.44c), a sample is assumed to be absorption-free. When considering the effect of the sample's linear absorption on the actual optical field strength, a modification is needed. The result is[45]

$$\chi^{(3)} = \left|\chi^{(3)}_{CS_2}\right| \left|\frac{I_{sample}}{I_{CS_2}}\right|^{\frac{1}{2}} \left(\frac{n_{sample}}{n_{CS_2}}\right)^2 \left(\frac{l_{CS_2}}{l_{sample}}\right) \frac{A}{\left(1-e^{-A}\right)e^{-\frac{A}{2}}}. \tag{3.4}$$

Here, n is the linear index of refraction, l is the sample path length (taken as the beam interaction length) and A is the absorbance at the working wavelength. Taking the sample path length as the beam interaction length is not a good assumption even for a very small angle. However, since our optical system configuration is kept the same for both reference and sample measurements, the ratio is in fact equal to unity.

To obtain the information about the solute's nonlinear optical property from the solution's, the simple additive theorem is adopted and the following relation is used:[45]

$$\chi^{(3)}_{solution} = L^4 (N_{solute}\gamma_{solute} + N_{solvent}\gamma_{solvent}). \tag{3.5}$$

Here, γ_{solute} and $\gamma_{solvent}$ stand for the second-order molecular hyperpolarizabilities, N_{solute} and $N_{solvent}$ represent the number of molecules per unit volume (cm^3) for the solute and solvent respectively, and L is the Lorentz local field factor. The reason for introducing the local field factor is that those individual molecules within a medium experience different electrical field strengths. This difference in the internal field is caused by the depolarization field, which originates from the polarization of all other molecules within the medium, along with the incident fields. The local field factor is very complicated, but for an isotropic nonpolar medium such as liquids and gases[7]

$$L^4 = \frac{\varepsilon+2}{3} = \frac{n^2+2}{3}, \tag{3.6}$$

where ε is the linear dielectric constant at the working frequency and n is the linear index of refraction. In writing $\varepsilon = n^2$, we assume that magnetic effects can be ignored.

For dilute solutions, Eq. (3.5) can be rewritten as

$$\chi^{(3)} = L^4 (N_{solute} \gamma_{solute}) + \chi^{(3)}_{solvent}. \tag{3.7}$$

Then from the plot of $\chi^{(3)}$ as a function of concentration, the second-order molecular hyperpolarizability, γ, for the solute can be determined.

Generally speaking, the third-order susceptibility $\chi^{(3)}$, or equivalently the second-order molecular hyperpolarizability, is a complex quantity. Its real and imaginary parts could be positive or negative. In the case where γ of the solute is a complex quantity and the solvent has only the real part, Eq. (3.7) yields the conjugate signal given by

$$\left|\chi^{(3)}_{eff.}\right|^2 = \left|L^4\left[N_{solute}\gamma^{Re}_{solute}\right] + \chi^{(3)}_{solvent}\right|^2 + \left|L^4 N_{solute}\gamma^{Im}_{solute}\right|^2. \tag{3.8}$$

The measured $\chi^{(3)}$ is an average value of the different elements for the $\chi^{(3)}$. In our case, the two pump and the probe beams are all parallel to the y-axis. The resulting conjugate wave has the same polarization direction as the probe beam. The various states of polarization of the conjugate wave for specific combinations of pump and probe wave polarizations, as well as the contributions from different elements, are listed in Table 3.1.[33]

As can be seen from the Table 3.1, for our experimental setup the measured $\chi^{(3)}$ value, some times called the effective third-order susceptibility, has the contribution from the $\chi^{(3)}$ tensor elements of $\chi^{(3)}_{xxyy}$, $\chi^{(3)}_{xyxy}$ and $\chi^{(3)}_{xyyx}$, as well as the degenerate elements[33]:

$$\chi^{(3)}_{eff.} = \frac{3}{2}\left[\chi^{(3)}_{xxyy}\cos\theta + \chi^{(3)}_{xyyx}\right]. \tag{3.9}$$

For very small θ, $\cos\theta \approx 1$. What is then measured is $\chi^{(3)}_{xxxx}$. As a comparison, the third-order harmonic generation (THF) measures the quantity[46]

$$\chi^{(3)}_{eff.} = \frac{1}{5}\left[3\chi^{(3)}_{xxxx} + 6\chi^{(3)}_{xxyy}\right]. \tag{3.10}$$

3.4 Calibration of the System and Reliability of the Results

In the DFWM experiment, the reliability of the data needs to be dealt with carefully. Usually the measured $\chi^{(3)}$ has contributions from the purely electronic

TABLE 3.1 Wave Polarization Directions in Degenerat Four-wave Mixing

E_f	E_b	E_p	E_c	Amplitude
x'	x'	x	x	$\frac{C'+C''+D}{4} A_f A_b A_p^*$
x'	x'	y	y	$\frac{D}{4} A_f A_b A_p^*$
y'	y'	x	x	$\frac{D}{4} A_f A_b A_p^*$
y'	y'	y	y	$\frac{(C'+C'')\cos^2\theta+D}{4} A_f A_b A_p^*$
x'	y'	ax + by $(a^2 + b^2) = 1$	$\left(\frac{a(C'+C''+D)x+bDy}{\sqrt{a^2(C'+C''+D)^2 + b^2D^2}}\right)$	Independent of θ
y'	y'	ax + by	$\left(\frac{aDx+b\left[(C'+C'')\cos^2\theta + D\right]y}{\sqrt{a^2D^2 + b^2\left[(C'+C'')\cos^2\theta + D\right]^2}}\right)$	Depends on θ
x'	y'	ax + by	$\frac{bC''x+aC'y}{\sqrt{b^2C''^2+a^2C'^2}}$	$\frac{1}{4}\sqrt{a^2C'^2+b^2C''^2}\cos\theta A_f A_b A_p^*$
$\frac{x'+y'}{\sqrt{2}}$	$\frac{x'-iy'}{\sqrt{2}}$	ax + by	$\frac{ax+b\cos^2\vartheta}{\sqrt{a^2 + b^2\cos^2\theta}}$ [b]	depends on θ

[a]For transparent nonresonant media, $C' = C'' = 3(\chi_{xxyy} + \chi_{xyxy})$, $D = 6\chi_{xyyx}$.

[b]For C' = C"

The geometry of DFWM

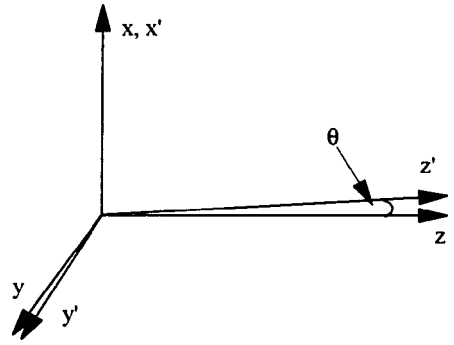

Adopted from "Nonlinear Optical Parametric Processes in Liquid and Gases" by J.F.Reintjes, Academic, Orlando, 1984, page 370

nonlinearity, the vibration nonlinearity, and the thermal effect. The thermal effect may come from ultrasonic phonon modulation and/or the reflection of the probe wave from the thermal gratings formed by two counter-traveling pump waves. Distinguishing the various sources that contribute to the measured $\chi^{(3)}_{eff.}$ is rather difficult. Fortunately, the response time for these processes is different, and this difference in response time can be used as a way to distinguish the sources.[47] The electronic nonlinearity has a response time less than 10^{-12} seconds. The vibrational response time is around 10^{-12} seconds in the resonant case. The reorientational response time for an anisotropic fluid is longer than 10^{-12} seconds, and the thermal effect time domain is longer than 10^{-9} seconds for ultrasonic phonon modulation and longer than 10^{-6} seconds for the thermal grating.

Our laser pulse width is 20 ns, which is within the response time domain for the thermal effect. Nevertheless, whether the thermal effect contributes much to the measured $\chi^{(3)}_{eff.}$ depends on the linear absorption of the sample solution at the working wavelength. The comparison is made of the $\chi^{(3)}$ for CS_2 measured in our work to the published data that are obtained from a DFWM with 20 ps pulse width laser source.[48] We use THF as solvent and measure the $\chi^{(3)}$ at different CS_2 concentrations. The result is shown in Figure 3.5. It should be pointed out that the procedure here is a relative measurement.

As can be seen from the Figure 3.5, the correlation of the $\chi^{(3)}$ and the solution concentration is very good with a coefficient of confidence of 0.9974. The $\chi^{(3)}_{CS_2}$ obtained from Fig. 3.7 is 7.6×10^{-13} esu, with an uncertainty range of less than 16%. Compared with the $\chi^{(3)}_{CS_2}$ value of 6.8×10^{-13}esu, our result is about 12% larger. In fact, the measured $\chi^{(3)}$ value is 48% larger than the accepted value of 5×10^{-13}esu for CS_2 by one of the authors of the reference 48, where a laser with pulse width narrower than 4 ps was used.[47] This clearly shows the effect of the laser pulse width on the measured $\chi^{(3)}$ value.

The minimized thermal effect in our experiment can be explained as the result of no linear absorption at the working wavelength. All of our sample solutions as well as CS_2 do not appear to have any significant absorption near the working wavelength of

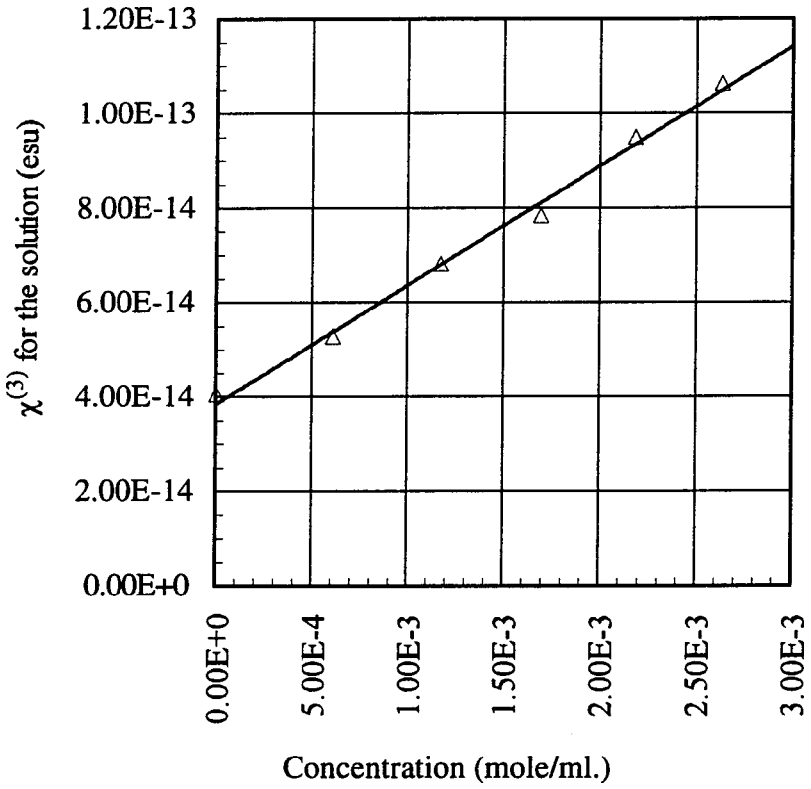

Figure 3.5 $\chi^{(3)}$ value of CS_2 as a function of concentration. Using CS_2 as solute and THF as solvent, we measure the $\chi^{(3)}$ value for CS_2. The uncertainty is less than 16%; the coefficient of confidence for the curve fitting is 0.9974

532 nm. Figure 3.6 shows the absorption spectrum for CS_2 and THF. Therefore, the measured $\chi^{(3)}$s are considered to mainly be determined by the electronic and reorientation nonlinearity for our nonpolar isotropic solutions.

Unless an ultrafast sub-pS laser is used, there is no easy way to distinguish the effects of the electronic nonlinearity from the reorientational contribution. In principle, the reorientational effect depends heavily on the sample molecule size. Bigger molecules need more reaction time to reorient to the polarization of the incident optical field and the relaxation time is also longer. Bigger molecules may have a relatively larger part of their measured second-order molecular hyperpolarizabilities coming from the reorientational contribution when a long pulse laser is used. For small molecules, this reorientation effect is smaller.

The stability of degenerate four-wave mixing, that is, whether repeated measurements yield a consistent result, is another concern. Figure 3.7 shows repeatedly measured $\chi^{(3)}$ for CS_2 during a time of four hours. The maximum shift of the $\chi^{(3)}$ for CS_2 from Fig. 3.9 is less than 3%. Thus, the short time reliability of our experiment is good. Of course, whenever a group of results is believed to be not reliable, especially when the $\chi^{(3)}$ values for CS_2 measured at the beginning and the end of the experiment differ by too much, the whole group of the data will be rejected.

The long term reliability is checked by examining the $\chi^{(3)}$ values for the solvent THF. Since THF is used as the solvent and its $\chi^{(3)}$ value is measured each time a sample's $\chi^{(3)}$ value is measured, we have the opportunity of checking the consistency in our experiment. The experimental conditions, like laser output power and the optical path alignment, are not exactly the same for these repeatedly taken $\chi^{(3)}$ values for THF.

Nevertheless, the average value for THF is $\chi^{(3)}_{THF} = 4.5 \times 10^{-14}$esu with a standard deviation of 35%, which is larger than our experiment uncertainty of 26%. The reported $\chi^{(3)}$ values for THF by other research groups are mostly in the range of 10^{-14} esu and have a positive real part.[41]

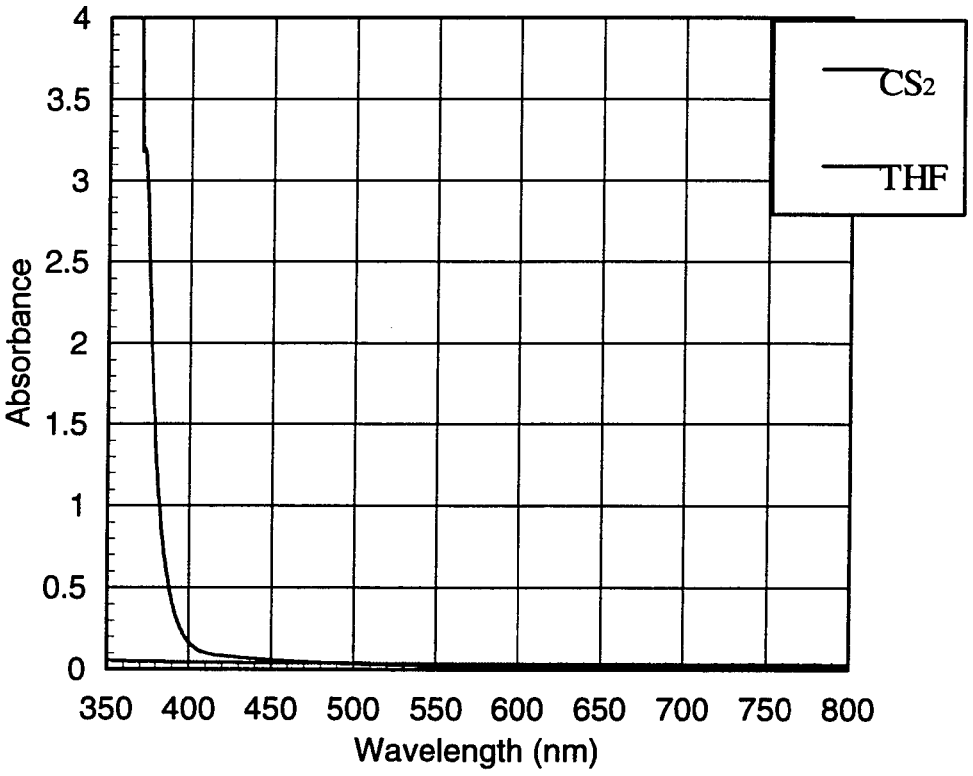

Figure 3.6 The absorbances for Pure CS_2 and THF. The sample cell is a 10-mm quartz cell. There is an absorption peak at around 350 nm for CS_2

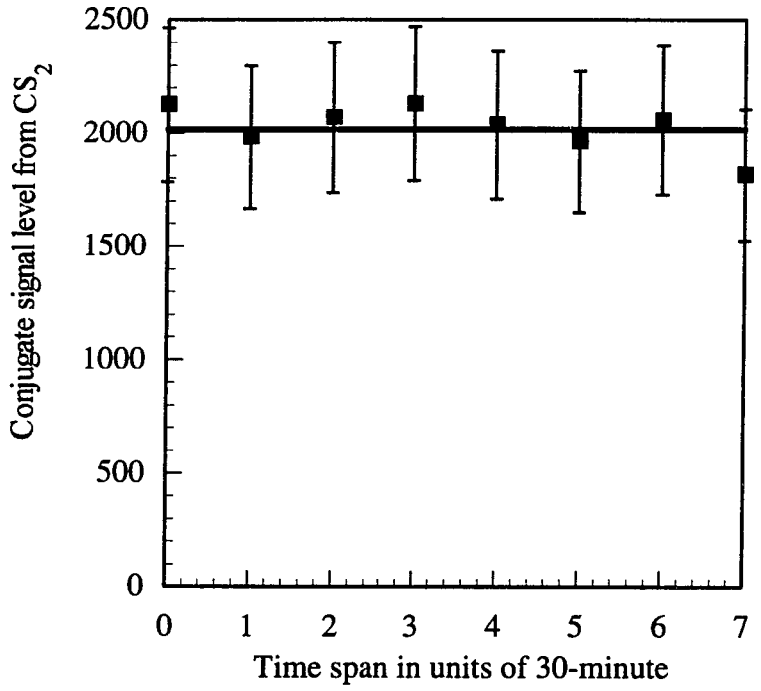

Figure 3.7 Short-term stability of the DFWM system. The y-axis is the conjugate signal level from a solution of pure CS. The x-axis is time in units of 30 min./division

In our data processing, $\chi^{(3)} = 6.8 \times 10^{-13}$esu for CS_2 is adopted from reference 48. The indexes of refraction for sample solutions at different concentrations are taken as the same as the solvent, $n_{CS_2} = 1.627$ for CS_2, n = 1.407 for THF and n = 1.424 for CH_2Cl_2.[49] We measured the index of refraction, n, as a function of the sample concentration for several types of samples on a Double Beam Differential Refractometer (model DRM - 1020, made by Otsuka Electronics).

The results are $dn/dc = 0.1244$ ml/gm for complex $Mo(CO)_5(PPh_3)$ and $dn/dc = 0.1991$ ml/gm for complex $Mo(CO)_4(PPh_2COMe)_2$. The error brought into the final γ values by using the solvent's index of refraction value instead of actual sample solutions' index of refraction value at the working concentrations is less than 1%. This error is negligible when compared to the experiment data uncertainty.

The absorbances of the sample solutions are measured on a UV-VIS spectrophotometer (model Response-I, made by Gilford) with the scan wavelength range from 350 nm to 800 nm and a quartz sample cell of 10 mm depth. All samples present little or no linear absorption at our DFWM working wavelength. Thus, in the data processing, the absorption correction factor is taken as unity.

The uncertainty level for the experimental results extends from 16% to 26%. We also notice that the reference solution, CS_2, has the strongest reflected conjugate signal and the ratio of the standard deviation to the mean value for CS_2 is the smallest at 16%. It is found that the uncertainty is higher for those samples with a small γ value (weaker conjugate signal) and much lower for the samples emitting relatively stronger conjugate signals, such as CS_2.

During our experiment, a group of neutral density filters is put in front of the detector to keep the conjugate signal detector (photo diodes) working within its optimal intensity range. The largest filtering factor in our experiment is around 10^3 for very strong conjugate signals. For the weak conjugate signal, there is no filtering at all. This may suggest that the increasing uncertainty for sample solutions of weak conjugate signal is

partially due to the nonuniform damping characteristic of the neutral filters. The weak optical background noise is not filtered out as efficiently for the small filtering factor as for large filtering factor. Since the output from the signal peak detector photo diode has a relatively narrow range, the electronic equipment parameters usually are the same. Thus, the uncertainty caused in by the electronic background should be same for all measurements.

CHAPTER 4

RESULTS AND ANALYSIS

4.1 Some Recent Experimental Results

Most studies of materials for third-order nonlinear optics applications have focused on conjugated organic compounds because it is well established that they exhibit large third-order nonlinearities. Conjugated polymers with nonresonant second-order molecular hyperpolarizabilities, γ, larger than 140×10^{-34} esu (corresponding to a $\chi^{(3)}$ value of about 10^{-7} esu) have been reported.[50,51]

There has recently been interest in metal organic complexes as third-order nonlinear optical materials because these complexes can also have highly conjugated structures. Some recently published experimental γ values for some of these metal complexes and some comparable organic materials are listed in Table 4.1. The molecular structures for the materials in Table 4.1 are given in Figure 4.1. The γ values for complexes 1, 2, 4, and 6 are believed, by the respective authors, to have resonant enhancement through either one-photon or two-photon absorption. The optical responses for the other compounds are nonresonant.

The metal complexes in Figure 4.1 exhibit a variety of conjugated structures. Compound 1 is a planar complex with a highly conjugated porphyrin ligand. Compound 2 is related to 1 but is not a metal complex. Compounds 3 and 4 are also conjugated and contain a ferrocene complex in which a cyclopentadienyl group is π-bonded to an iron(II). Compound 6 has a unique structure in which two planar, conjugated phthalocyanine ligands are bridged by a lutetium(IV). It is obvious that resonant enhancement is a very

TABLE 4.1 Some Recently Reported γ Values

#	Name	$\langle\gamma\rangle \times 10^{-34}$ esu	Method
1	zinc-meso-tetra-(*p*-dimethylaminohenyl)tetrabenzporphrine[52]	100000.	DFWM
2	tetrabenzporphyrin[52]	50000.	DFWM
3	ferrocene[48]	0.161	DFWM
4	1,1"-(1,4-phenylenedi-2,1-ethenedily)bis(ferrocene)[48]	2.70	DFWM
5	DPH[27]	120.	DFWM
6	$LuPc_2$-bis(phthalocyanines)[53]	3400.	DFWM
7	PPQ[54]	1.5	THG
8	C_6H_6[55]	0.0385	THG

The large measured γ values for complexes 1, 2, 4, and 6 are believed by the respective authors to have the resonant enhancement through either one-photon or two-photon absorption processes.

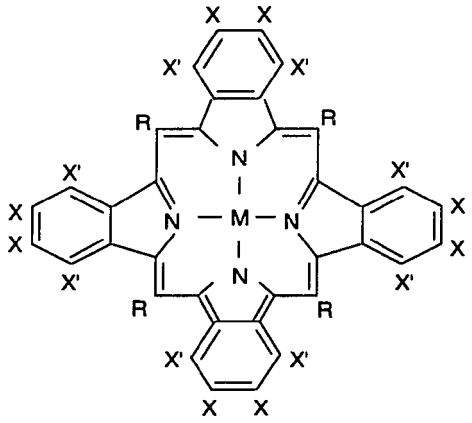

1. x = x' = H, M = Zn^{2+},
   R = *p*-Dimethylaminophenyl
2. x = x' = H, M = two-H,
   R = H

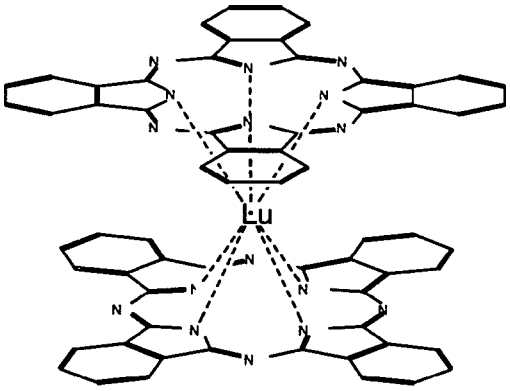

6. $LuPc_2$-bis(phthalocyanines)

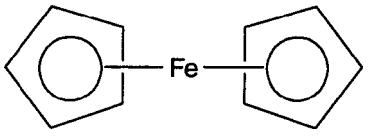

3. Ferrocene

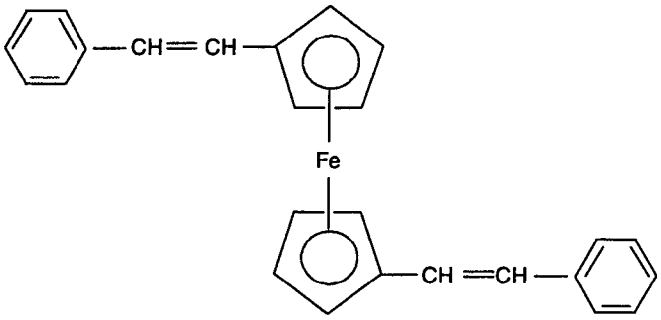

4. 1,1"-(1,4-phenylenedi-2,1-ethenediyl)bisferrocene

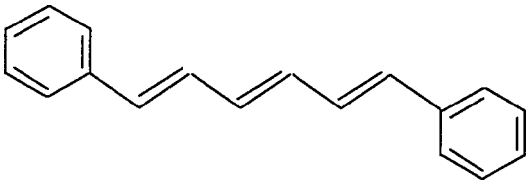

5. diphenylhexatriene

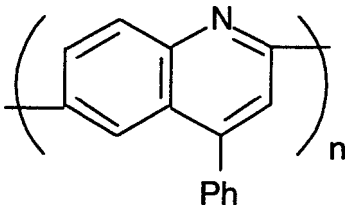

7. PPQ

Figure 4.1 The molecular structure of some one- and two-dimension polymers and metal-organic materials

important factor in determining the magnitude of γ in metal complexes. It is less clear what other factors are affecting the magnitude of γ in these complexes.

In organic materials it is well established that, in addition to a large effective conjugation length, a high concentration of easily polarizable electrons also increases the third-order optical nonlinearity.[56] As the conjugation length increases, the electrons are less tightly bound, thus making them more easily polarized through interaction with the optical field. The small optical band gap of the organic materials is also important for a medium to have a fast response time. This is a property that solid-state inorganic materials lack.[57] It not clear, however, whether these factors also affect the third-order optical nonlinearities of metal complexes. To determine which factors do affect the third-order optical nonlinearities of metal organic complexes it is necessary to study a series of closely related complexes in which resonant enhancement does not occur. We have done this for transition metal complexes with phosphorus-donor ligands, and our results are presented below.

4.2 Second-Order Molecular Hyperpolarizabilities of Transition Metal Complexes

The transition metal complexes and their spatially averaged $\langle\gamma\rangle$ values are given in Table 4.2. Because of difficulties in accurately determining the sign of the real part of the $\langle\gamma\rangle$ values from DFWM experiments, no signs are given. Several plots of $\chi^{(3)}$ values of the solution as a function of concentration are shown in Figures 4.2 and 4.3.

Most of the samples that we have studied are molybdenum (Mo) complexes with d^6 electron configurations. Other samples are platinum (Pt), palladium (Pd), and rhodium (Rh) complexes with d^8 configurations, and a tungsten (W) complex with a d^6 configuration. We have also studied two phosphorous ligands, $OPPh_3$ and PPh_3, for comparison. The complexes and ligands were chosen because both the metal and the number and type of ligands are different. Themeasured molecular hyperpolarizabilities (γ) for these complexes vary over three orders of magnitude, from the largest value of

TABLE 4.2 The Second-order Molecular Hyperpolarizabilities, γ, for Some Transition Metal Organic Complexes

	Complex Name	$\langle\gamma\rangle \times 10^{-34}$
1	PPh_3	2.9
2	$OPPh_3$	1.5
3	*cis*-$Mo(CO)_4(PPh_3)_2$	1700.0
4	*trans*-$Mo(CO)_4(PPh_3)_2$	330.0
5#	$Mo(CO)_5(PPh_3)$	1.5
6	*cis*-$Mo(CO)_4(PPh_2NHMe)_2$	270.0
7	$Mo(CO)_5(PPh_2NHMe)$	6.0
8#	$Mo(CO)_5(PPh_2NH_2)$	8.6
9	*cis*-$Mo(CO)_4(PPh_2COMe)_2$	260.0
10#	*cis*-$Mo(CO)_4(PPh_2OMe)_2$	44.0
11	*cis*-$Mo(CO)_4(PPh_2Cl)_2$	14.0
12#	*cis*-$Mo(CO)_4(PPh_2Me)_2$	4.0
13	*cis*-$Mo(CO)_4(PPh_2CH_2Ph)_2$	630.0
14	*cis*-$Mo(CO)_4(PPhthiophene_2)_2$	350.0

TABLE 4.2 The Second-order Molecular Hyperpolarizability γ for Some Transition Metal Organic Complexes
(Continued)

15	$Mo(CO)_4(PPh_2O)_2Si$ (Bu^t, Me)	39.0
16	$Mo(CO)_4$ (PPh_2 - NH, CH_2, NMe_2 - CH_2)	440.0
17*#	*cis*-$PtCl_2(PPh_2$thiophene$)_2$	1900.0
18*	*trans*-$PdCl_2(PPh_3)_2$	140.0
19	*trans*-$PdCl_2(PPh$thiophene$_2)_2$	670.0
20	$Rh(CO)_2$(acac)	1.7
21	$W(CO)_4$ (PPh_2 - O, CH_2, NMe_2 - CH_2)	7.0

The absorbances for all sample are smaller than 0.1, or absorption coefficient, αs, are smaller than 0.1 cm^{-1}, at the wavelength of 532 nm and at a concentration of around 0.01 Mole./lit. The nearest absorption peak is at about 350 nm wavelength. The samples with a "*" use CH_2Cl_2 as solvent. The γ value of the samples with a "#" possibly have a negative real part.

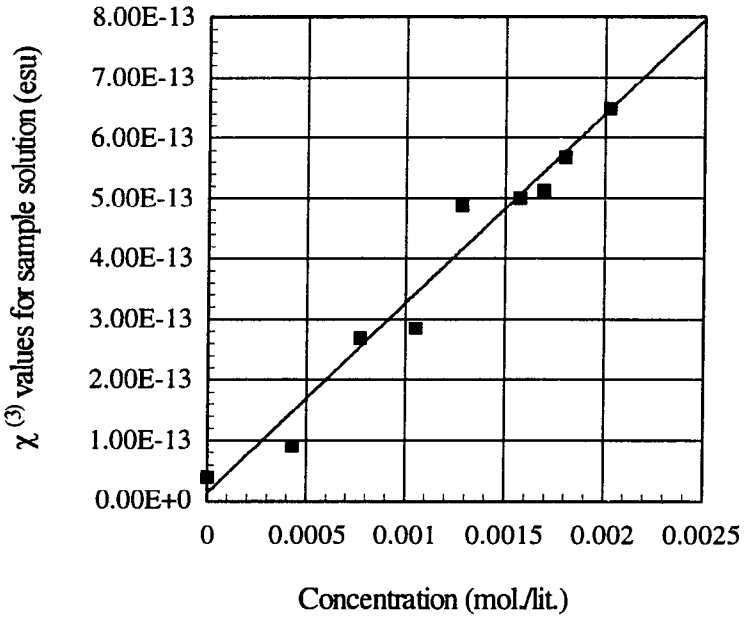

Figure 4.2 DFWM $\chi^{(3)}$ values versus concentration curve for complex *cis*-$Mo(CO)_4(PPh_3)_2$. The solvent is THF. The linear coefficient of confidence r = 0.9594

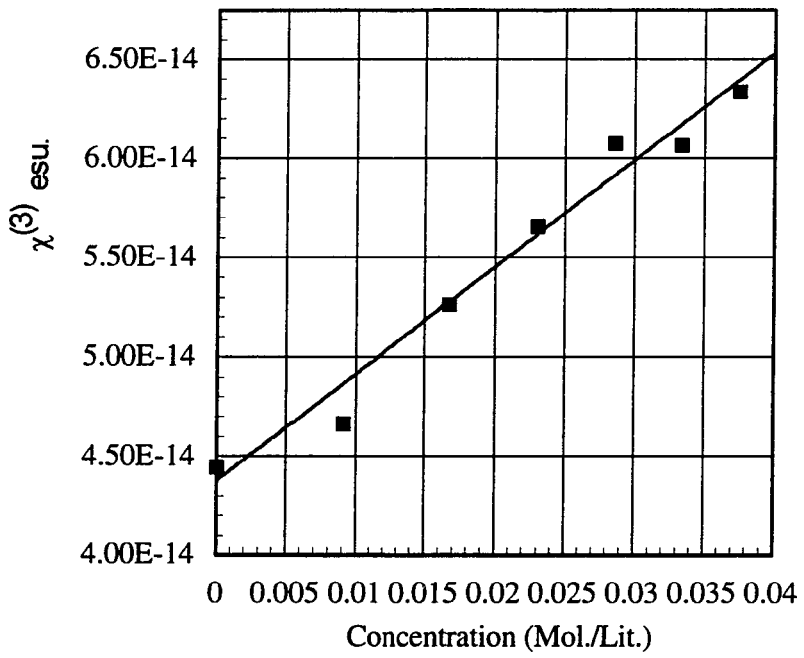

Figure 4.3 The dependence of PPh_3 solution $\chi^{(3)}$ values on the concentration. The solvent is THF. The linear coefficient of confidence r = 0.9867

1900×10^{-34} esu for *cis*-$PtCl_2(PPh_2thiophene)_2$ to the smallest values of 1.5×10^{-34} esu for $Mo(CO)_5PPh_3$ and $OPPh_3$.

As mentioned earlier, the nonlinear optical properties for organic complexes are believed to be largely due to π electron delocalization. A conjugated structure, in which π electrons can move over entire length of the molecule, is the most favorable for a large nonlinearity. However, a conjugated structure does not necessarily ensure a large third-order nonlinearity. For example, benzene, with a perfectly conjugated structure, has a second-order molecular hyperpolarizability, γ, of only 6×10^{-36} esu.[58] As is the case in semiconductor materials where the number of the free carriers has the major role on the nonlinear optical property,[59-61] the ability to supply and accept π electron between different components within an organic molecule is as important as the extended conjugate length.

We choose the complexes shown in Table 4.2 for this study because they have both donor (phosphorus-donor ligands) and acceptor (carbonyl ligands) groups potentially conjugated by overlap of the metal d orbitals with d orbitals on the phosphorus and with π^*-orbitals on the carbonyls. The σ-donation of unshared pair of electrons in an sp^3 orbital on phosphorus into empty dsp hybrid orbitals on the metal should produce a large electric dipole momentum in the complex that could result in a large nonlinear optical response to the incident light. This response could be enhanced in the carbonyl complexes by donation of electron density from filled t_{2g} d orbitals on the metal into empty π^*-orbitals on the carbonyl ligands. Thus, it seemed possible that these complexes might exhibit large second-order molecular hyperpolarizabilities. In addition, the phosphorus donor ligands in these complexes were closely related, and this would allow the effects of different substituents on the phosphorus-donor ligands on the second-order hyperpolarizabilities to be determined. Finally, these complexes have no linear absorption at the wavelength of interest in contrast to may of the other complexes which are reported in Table 4.1. Thus,

we do not need to be concerned with resonant enhancement of the second-order molecular hyperpolarizabilities in these complexes.

4.3 Factors Affecting γ Values of Mo Complexes

The second-order molecular hyperpolarizabilities of the $Mo(CO)_{6-n}(Ph_2PX)_n$ (n = 1, 2) complexes are affected by the number and arrangement of the phosphorus-donor ligands about the molybdenum and by the nature of the X substituent of the phosphorus-donor ligand. The molecular structures and the measured γ values for some samples are shown in Figure 4.4. The effects are interrelated and are discussed below.

The coordination geometry of the complex has a significant effect on its γ. The γ of $Mo(CO)_5(PPh_3)$ (1.5×10^{-34} esu) is similar to those of PPh_3 (2.9×10^{-34} esu) and $OPPh_3$ (1.5×10^{-34} esu) and is several orders of magnitude less than those of *cis*-$Mo(CO)_4(PPh_3)_2$ (1700×10^{-34} esu) and *trans*-$Mo(CO)_4(PPh_3)_2$ (330×10^{-34} esu). These results are not consistent with the model based on bonding in these complexes proposed above because the γs exhibited by the free, oxidized PPh_3 group coordinated to the $Mo(CO)_5$ are essentially the same. Also, it does not seem possible to explain this behavior based upon Eq. (2.28). When the optical field frequencies are far away from the medium's resonance frequency, as is true for these complexes, the denominator changes little and the major contribution to the γ value is from the speculative value of the electrical dipole integrations $(r)_{xy}$s. More extended charge separations result in larger products for the electric dipole momentum that, in turn, yield larger γ value for the complexes. Thus, increasing the length of the dipole should result in an increase in γ. However, in the series of $Mo(CO)_{6-n}(PPh_3)_2$ (n = 1, 2) that are reported in Table 4.2, the γ for the trans, disubstituted complex, which does not have a permanent dipole, is two orders of magnitude greater than that for the monosubstituted complex. A possible explanation for this behavior will be given below.

The X substituents on the phosphorus-donor ligands in $Mo(CO)_{6-n}(Ph_2PX)_n$ (n = 1, 2(cis)) also have unusual effects on the γs of these complexes, and these effects appear to

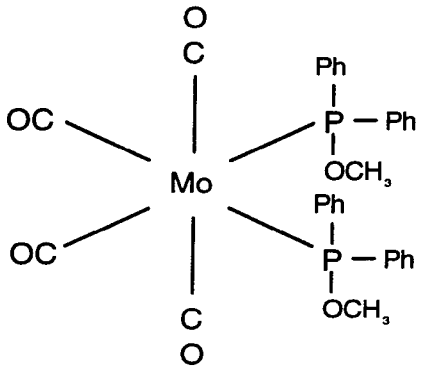

$\gamma = 44 \times 10^{-34}$ esu

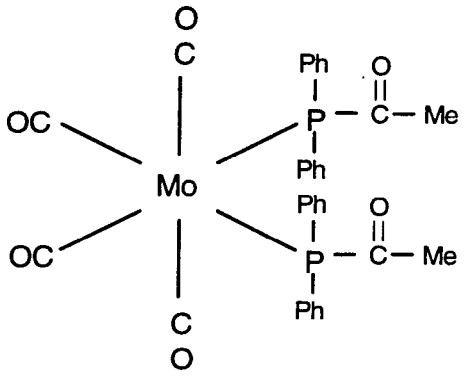

$\gamma = 260 \times 10^{-34}$ esu

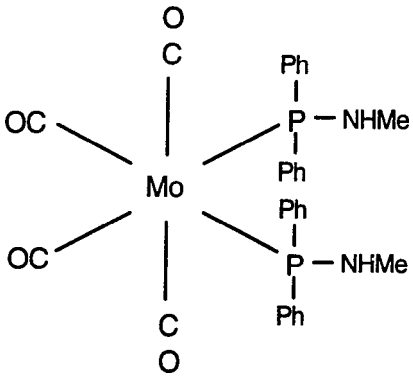

$\gamma = 270 \times 10^{-34}$ esu

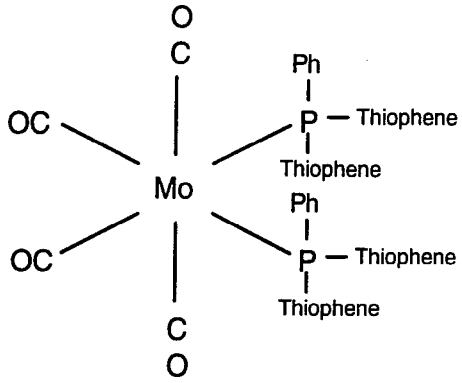

$\gamma = 350 \times 10^{-34}$ esu

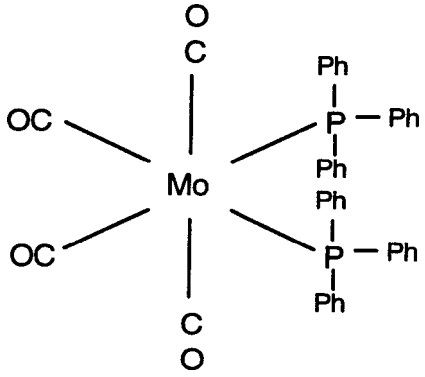

$\gamma = 1700 \times 10^{-34}$ esu

Figure 4.4 Some Mo complexes molecular structures and their γ values. The difference in γ values is caused by the ligands

depend on the coordination geometries of the complexes. Variation in the X substituent in the monosubstituted (n = 1) complexes has little effect on the γ of the complex with $Mo(CO)_5(PPh_2NH_2)$ exhibiting the largest γ (8.6×10^{-34} esu) and $Mo(CO)_5(PPh_3)$ exhibiting the smallest γ (1.5×10^{-34} esu). In contrast, variation in the X substituent in the cis disubstituted (n = 2) complexes has a very large effect on the γ with *cis*-$Mo(CO)_4(PPh_3)_2$ exhibiting the largest γ (1700×10^{-34} esu) and *cis*-$Mo(CO)_4(PPh_2Me)_2$ exhibiting the smallest γ (4.0×10^{-34} esu). This order cannot be explained by variations in the electron donor abilities of the phosphorus-donor ligands. Nuclear magnetic resonance (NMR) and infrared (IR) spectroscopic studies of the $Mo(CO)_{6-n}(Ph_2PX)_n$ (n = 1, 2(cis)); X = Cl, Oalkyl, Oaryl, NHalkyl, NHaryl, alkyl) complexes have demonstrated that phosphine with alkyl substituents are the best electron donors.[62-68] Thus, if the electron donor ability of the phosphines was the factor determining the magnitude of γ, *cis*-$Mo(CO)_4(PPh_2Me)_2$ ($\gamma = 4.0 \times 10^{-34}$ esu) and *cis*-$Mo(CO)_4(PPh_2CH_2Ph)_2$ ($\gamma = 630 \times 10^{-34}$ esu) should have the largest γs. This is obviously not the case, implying that the electron donor ability of the phosphorus-donor ligand does not affect the γ of the complex.

A possible explanation for this behavior is that the magnitude of the optical nonlinearities of these complexes depends upon the number of phosphorus substituents that are capable of π-electron delocalization. This would explain why the complexes with the largest nonlinearities are those in which the X substitutents contain conjugated phenyl rings, *cis*- and *trans*-$Mo(CO)_4(PPh_3)_2$, and *cis*-$Mo(CO)_4(PPh_2CH_2Ph)_2$. Other complexes with large nonlinearities are those in which the X substituents are either thiophene or acetyl substituents, which also have π-systems, or amino groups, which can form pπ-dπ bonds between the phosphorus and the nitrogen. Complexes with small nonlinearities are those in which the X-substituents do not have π electrons such as alkoxy, silyloxy, chloride, and methyl groups.

There are two interesting aspects of the hypothesis above that need further explanation. The first is that the conjugated groups do not need to be directly bonded to the phosphorus to enhance the optical nonlinearity. Thus, the γ for *cis*-$Mo(CO)_4(PPh_3)_2$ is only three times that of *cis*-$Mo(CO)_4(PPh_2CH_2Ph)_2$ but 1000 times that of $Mo(CO)_5(PPh_3)$. The second is that the dipole of the molecule does seem to have some effect on its optical nonlinearity. Thus, the γ of *cis*-$Mo(CO)_4(PPh_3)_2$ is five times that of *trans*-$Mo(CO)_4(PPh_3)_2$.

It is of interest to determine the relationship between the number of groups with π -electrons and the third-order optical nonlinearities of the $Mo(CO)_{6-n}(PPh_2X)_n$ complexes. Two different relationships are shown in Figure 4.5. In Figure 4.5 (a), the common logarithms of the complexes' second-order molecular hyperpolarizabilities, γs, are plotted versus the number of groups with π-electrons in the complexes. The γ for benzene is included in this plot to give a baseline for a compound with a single aromatic ring. This gives a linear plot ($\gamma = A\,\mathbf{exp}(B \cdot n)$), with $A = 1.094 \times 10^{-36}$, $B = 1.86$, and the regression coefficient r = 0.9911. It is also possible carry out a power ($y=ax^b$) least-squares fitting on the average γ values at each of the π-electron containing groups, and this is shown in Figure 4.5(b). The regression results an exponent of b = 4.9985 with the regression coefficient r = 0.9706. It is of interest to compare this exponent value to a value of 5 predicted by the free-electron model for thiophene oligomers[23] where the γ value increases with the number of the repeat unit. The DFWM measurement of those oligomers gives an exponent of 4.[69,70] It should be noted that thiophene oligomers have a linear conjugated π electron structure, and the loosely bonded π electrons can move freely over the entire molecule. The similarity in the dependence of the γ values on a power form and the closeness of the exponents suggest that the π-electron-containing substituents in the Mo complexes, response to the incident laser light is like the free-moving π electrons in the linear conjugated thiophene oligomers. This is an extremely

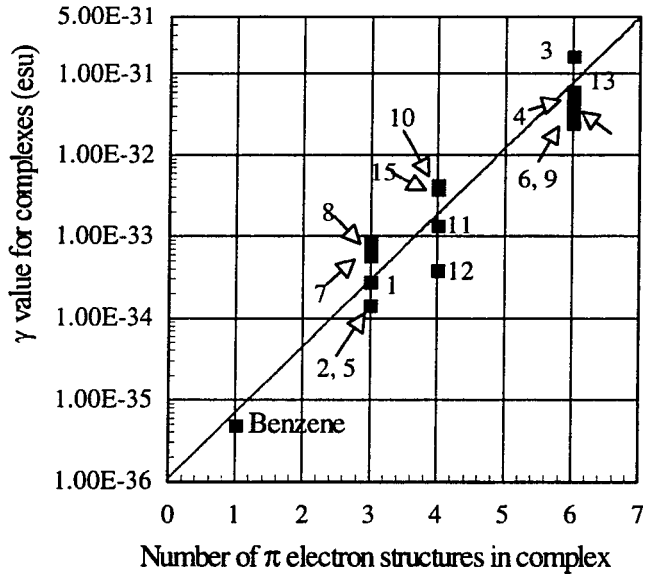

(a)

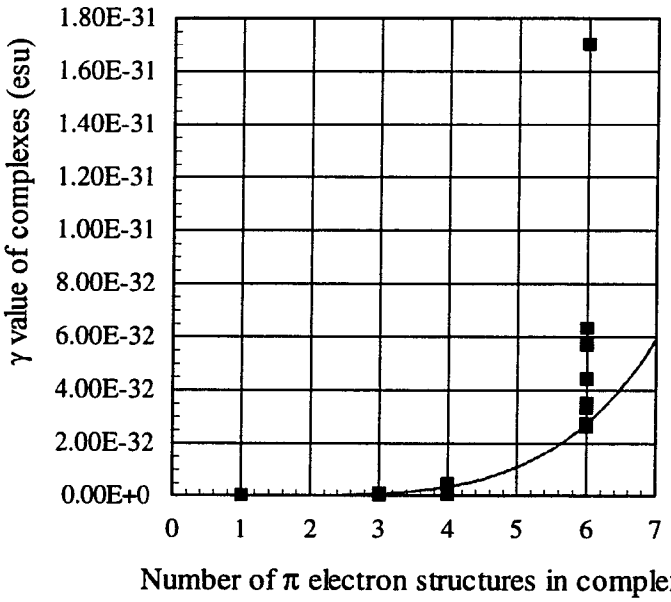

(b)

Figure 4.5 The power fitting of molecular hyperpolarizability as a function of the number of π electron structure in complexes. (a) Vertical axis is in the scale of $\log_{10}$. (b) The power form ($y = ax^b$) fitting gives $a = 3.5351 \times 10^{-36}$ esu and $b = 4.9985$. The fitting coefficient $r = 0.9706$

surprising result because in no sense can these groups be considered to be conjugated. It does raise the possibility that even larger γs could be obtained in complexes with more π-electron containing phosphine substituents.

4.4 The Role of the Transition Metal Atom and the Other Ligands in the Complexes

Based on the analysis on the effects of phosphine ligands and their coordination geometry on the third-order optical nonlinearities of these complexes, a tentative explanation for the third-order optical nonlinearities exhibited by the $Mo(CO)_{6-n}(PPh_2X)_n$ is as follows. First, the metal atom acts like a "bridge" between the groups containing π-electrons so that π-electron delocalization can occur. However, at the current time, it is not clear whether the π-electron delocalization in the complexes is through the metal atom or by direct ligand-ligand coupling. Second, the electric dipole of the complex created by the different electron donor/acceptor abilities of the phosphorus-donor and carbonyl ligands further enhances complex's nonlinear response towards the optical field.

Although the studies described in the previous section suggest that the metal center plays a role in determining the optical nonlinearities of the complexes, the exact nature of that role is unclear. In addition, the effect of the other ligands on the optical nonlinearities of the complexes in also unknown. In order to better understand these two factors, we have measured the optical nonlinearities in a complexes with different metal centers and with different ligands attached to the metals. These results are discussed below.

Two complexes that allow some comparison of the effects of the metal on the γ values are *cis*-$Mo(CO)_4(PPh_2NHCH_2CH_2NMe_2)$ and *cis*-$W(CO)_4(PPh_2OCH_2CH_2NMe_2)$. These complexes have similar molecular structures, shown in Figure 4.6, which consist of four carbonyl ligands, a phosphorus-donor group, and an amine with the phosphorus-donor group and the amine cis to each other. However, the γ of the molybdenum complex is nearly two orders of magnitude larger than that of the tungsten complex. It is tempting

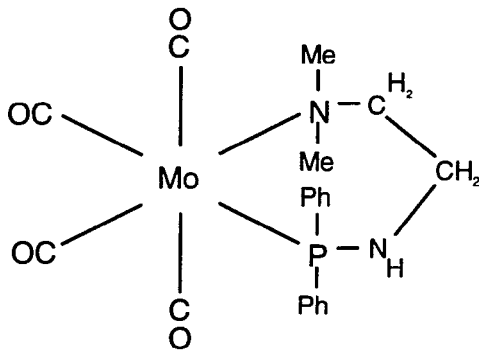

(a) $\gamma = 440 \times 10^{-34}$ esu

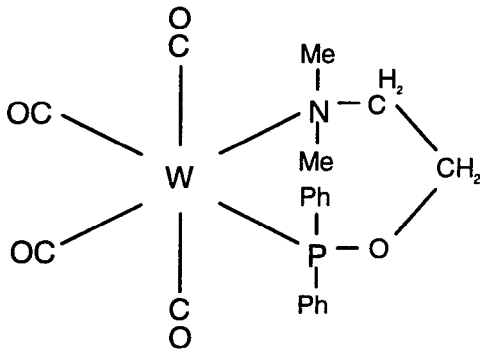

(b) $\gamma = 7.0 \times 10^{-34}$ esu

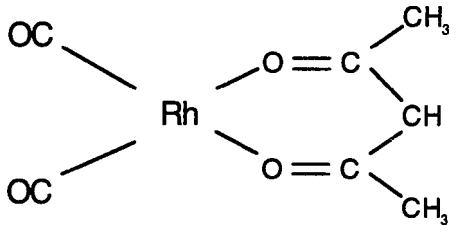

(c) $\gamma = 1.7 \times 10^{-34}$ esu

Figure 4.6 The effect of different transition metal atoms on the $\gamma^{(2)}$ values

to attribute this difference to the difference in the metal centers in the two complexes, and this would be consistent with literature results in which complexes of second row transition metals are reported to exhibit larger γs than those of third row elements.[53,71] However, some of the difference may also be due to the fact that phosphorus-donor group in the molybdenum complex is a phosphinamide while that in the tungsten complex is a phosphinite. Our studies of the $Mo(CO)_{6-n}(Ph_2PX)_n$ (n = 1, 2) complexes indicate that these complexes with phosphinamide ligands generally have significantly higher γs than do those with phosphinite ligands. Thus it is not possible to determine how much of the difference is due to the metal and how much to the ligand.

An interesting point that does need to be made is that the γ value for the molybdenum complex (440×10^{-34} esu) is by far the largest γ that we observed for any complex with a single P-donor ligand. This suggests that the amino group, which is a good σ electron donor, may be having a significant effect on the second-order susceptibility in this complexes. Thus, a promising area of research is studies of complexes containing both phosphorus-donor and amine ligands.

We measured γ for $Rh(CO)_2(acac)$, shown in Figure 4.6 (c), because this complex contains a π-electron system that extends over the two ligands and the Rh. We thought that this might results in a large γ. Instead, the γ value for the rhodium complex is the smallest we have measured at 1.7×10^{-34} esu. This low γ does not seem to be due to the rhodium because it is in group VIII of the same period as molybdenum. This confirms our earlier conclusion that an extended π-electron does not necessarily give rise to a large γ in a transition metal complex and is consistent with the small γs reported in Table 4.1 for ferrocene complexes. It may be that the lack a strong electron-donor ligand in the complex results a relatively smaller electrical dipole momentum and thus in a low γ.

The comparisons between the platinum complex and two palladium complexes are complicated because of the somewhat different ligands and different coordination geometries in the complexes. Surprisingly, the largest γ is observed for the platinum

complex even though platinum is a third row transition metal and palladium is a second row transition metal. It does not seem possible to attribute the larger γ value of the platinum complex to the phosphorus-donor ligand because it is larger than that of the palladium complexes in which the ligands have more phenyls and more thiophenes. It may be that the difference in the γ values is due to fact that the phosphorus-donor groups in the platinum complex is cis but those in both palladium complexes are trans. However, this does not explain the lack of any effect due to the metals. Obviously, this point requires further study.

4.5 The Sign of the Real Part of γ

We have not addressed the sign (positive or negative) of the real part of the measured second-order molecular hyperpolarizability which is related to the third-order susceptibility. There exist five complexes that appear to have negative γ values. This is based on the reported positive real part of the γ value for tetrahydrofuran (THF), which is the solvent for most of the samples except for the platinum and palladium complexes where methylene chloride (CH_2Cl_2) is the solvent. Figure 4.7 shows the $\chi^{(3)}$ value versus solution concentration for the *cis*-$Mo(CO)_4(PPh_2OMe)_2$ complex. It seems that the real part of the γ value for this complex is negative, though independent z-scan measurement of the same complex gives differing results.[72] It is not clear at this time whether other samples with relative large γ value have a negative real part, since the masking effect of the large nonlinear optical response may have washed out the sign due to the lack of data at very low concentrations.

The reason for negative real part of $\chi^{(3)}$ tensor elements is not understood at this time nor can we determine easily which molecules possess a negative or positive real part without carefully measuring samples' γ value at very low concentration.

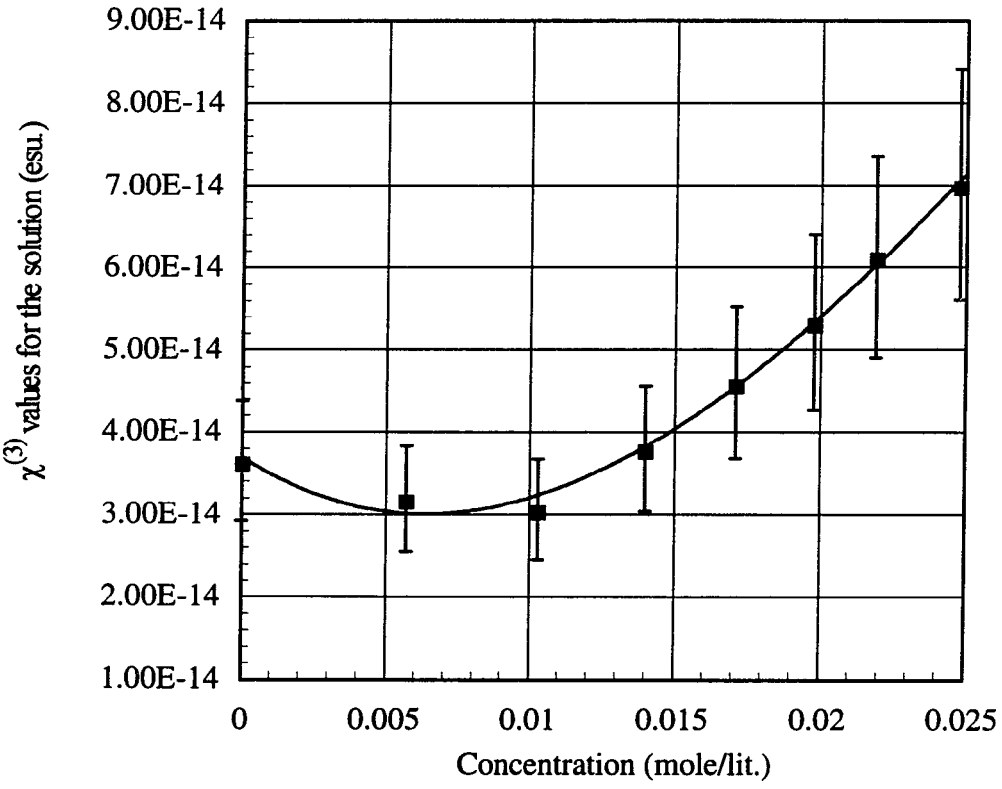

Figure 4.7 The dependence of sample *cis*-$Mo(CO)_4(PPh_2OMe)_2$ solution $\chi^{(3)}$ values on the concentration. The solvent is THF. From the curve shape, it can be determined that the real part of $\chi^{(3)}$ value for this complex is a negative number

We assume that the third-order nonlinear polarization $\mathbf{P}^{(3)}$ for a medium has the form of

$$P^{(3)} = \sum_i p_i^{(3)} = \sum_i LN_i\gamma_i E^3 \tag{4.1}$$

where the index i represents ith type of the molecule group, N_i is the number of ith group per unit volume, and γ_i is the second order molecular hyperpolarizabilty for the ith type group. For the sake of simplicity, we use the scalar form instead of vector form for the polarization and the tensor nature of γ is also replaced by a pure number. The substitution of Eq. 3.1 into Eq. 2.7, which describes the optical waves propagation inside a medium, gives

$$\frac{d^2E}{dz^2} - \frac{n_0}{c^2}\omega^2 E = \frac{4\pi\cdot 3\omega}{c^2} E^3 \sum LN_i\gamma_i + \frac{4\pi}{c^2}\frac{\partial^2 P^L}{\partial t^2} \tag{4.2}$$

with P^L being the linear polarization. It can be seen that the maximum nonlinear optical response will occur only when there is little or no cancellation among different molecule groups within a complex due to their positive or negative real parts of γ. From the view of wave propagation, this means all nonlinear responses must be in phase to get the enhanced result. This constraint is automatically satisfied in a system where the major contribution is from π-electron delocalization, since π electrons are supposed to behave like free-moving charge carriers. The reason for analyzing the sign of γ for the metal organic complex is to minimize the possible cancellation when choosing transition metal organic complexes, which may have a positive or negative real part of the γ, as the side groups to be attached upon a polymer backbone.

A possible explanation about the source of the negative sign for the real part of γ value is drawn from Eq. 2.28, the explicit expression for the $\chi^{(3)}$ tensor element. Because integration (r_{xy})s are the expected value of the bond length for dipoles, the numerators cannot be negative. So, the sign is determined only by the denominators which involved subtractions of term ω, 2ω, 3ω. (In degenerate four-wave mixing, all incoming waves have

a same frequency ω.) The denominators also have a bigger effect on the $\chi^{(3)}$ tensor element value if the frequency ω is near a transition frequency of the medium.

It can be seen clearly that the sign for the real part of the $\chi^{(3)}$ tensor element depends on how the medium energy levels are distributed and what is the incoming optical wave frequency. As to the resonant case, only one-photon and two-photon resonance could possibly give a negative sign.

Because little or no linear absorption presents at the working wavelength for all of the samples, one-photon resonance does not happen in our measurements. Table 4.3 shows the absorbance and the γ value for some of the samples. It can be seen from the Table that there is no correlation between the absorption and the measured third-order nonlinearity. Figure 4.8 shows a typical absorption spectroscopy for a molybdenum complex.

To investigate possible two-photon process, we have also measured the dependence of the DFWM conjugate signal intensity on the input laser power density for carbon disulphide (CS_2) and the molybdenum complex *cis*-$Mo(CO)_4(PPh_3)_2$. The results are presented in Figures 4.9 and 4.10. As can be seen from the figures, the ratio of the conjugate signal to the cube of input laser intensity remains constant when the laser power changes. The power ($y = ax^b$) fittings of the conjugate signal intensity versus reference intensity yield an exponent b slightly larger than 3, b = 3.1412 for CS_2 and b = 3.0376 for *cis*-$Mo(CO)_4(PPh_3)_2$. This leads us to believe that no two-photon resonance occurs. The conclusion is based on the theory[73] that two-photon absorption will cause conjugate signal intensity to be proportional to the fifth power of the incident intensity (I^5) instead of the cube of the incident intensity (I^3) for the nonresonant case.

From the discussion of the sign of the real part of $\chi^{(3)}$ tensor element, it is believed that there is little one or multi-photon resonance enhancement to the experiment results. And multi-photon (three-photon or above) resonance is the characteristic phenomenon of

TABLE 4.3 The Absorbance and Measured $\langle\gamma\rangle$ Values for Some Samples

Complex Name	Absorbance	$\langle\gamma\rangle \times 10^{-34}$ (esu)
cis-$Mo(CO)_4(PPh_3)_2$	0.0343	1700.0
trans-$Mo(CO)_4(PPh_3)_2$	0.1019	330.0
cis-$Mo(CO)_4(PPh_2NHMe)_2$	0.0293	270.0
$Mo(CO)_5(PPh_2NHMe)$	0.0137	6.0
$Mo(CO)_5(PPh_2NH_2)$	0.0373	8.6
cis-$Mo(CO)_4(PPh_2COMe)_2$	0.0855	260.0
cis-$Mo(CO)_4(PPh_2OMe)_2$	0.0173	44.0
cis-$Mo(CO)_4(PPh_2Me)_2$	0.0494	4.0

The absorbances are measured in a sample cell of a thickness of 10 mm and the sample concentrations are the same as those for DFWM measurement.

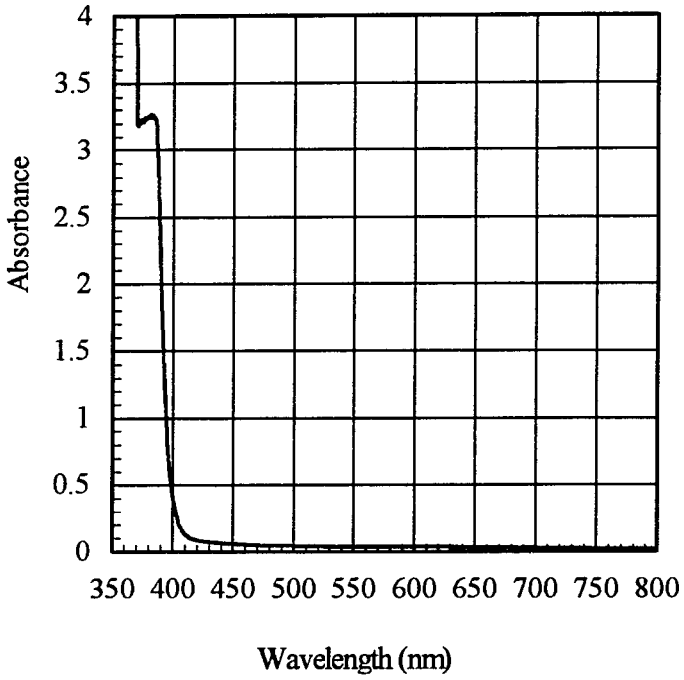

Figure 4.8 The absorption spectroscopy for complex *cis*-$Mo(CO)_4(PPh_3)_2$. The solvent is THF, and the concentration is 0.0248 mol./lit. The absorbance at 532 nm is less than 0.1, or the absorption coefficient α is smaller than 0.1 cm^{-1}

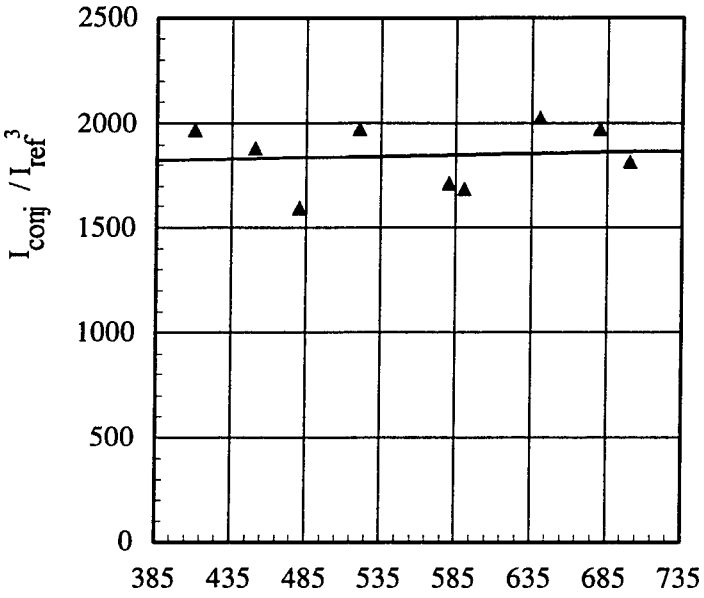

(a)

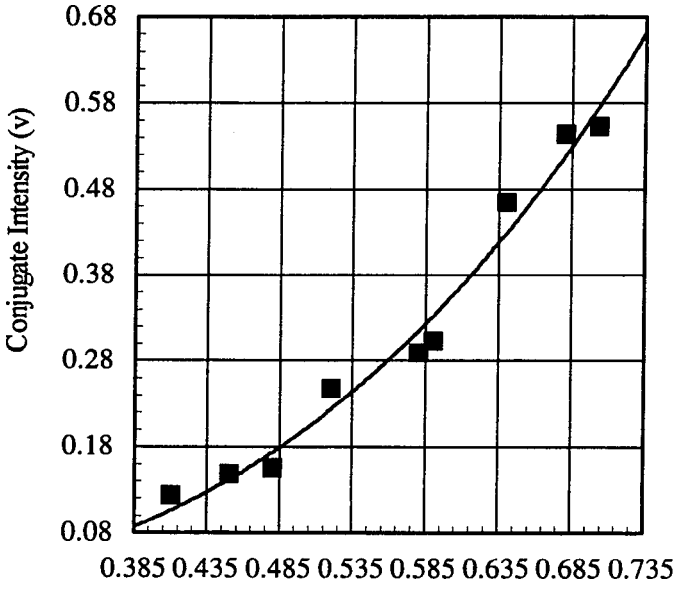

(b)

Figure 4.9 Conjugate signal as a function of laser intensity for CS_2. (a) The y-axis is the ratio of conjugate signal intensity over the cube of the reference signal intensity for CS_2. (b) The y-axis is conjugate signal intensity. The power curve ($y = ax^b$) fitting yields b = 3.1412 and r = 0.9773

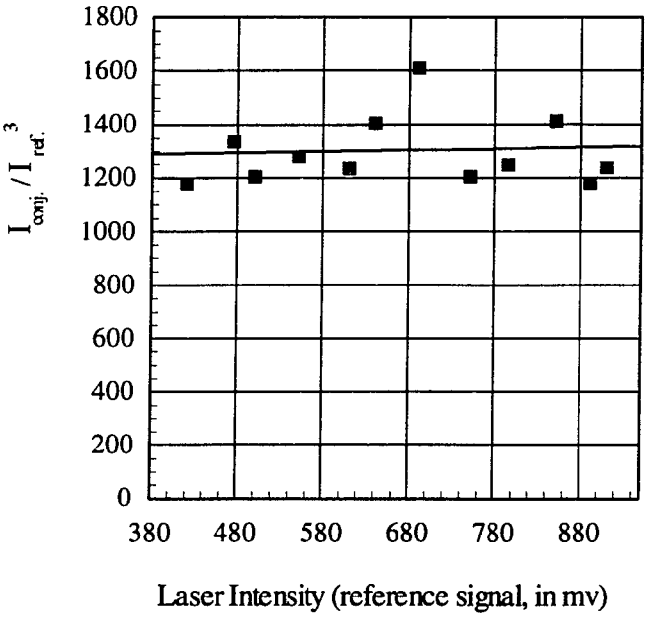

(a)

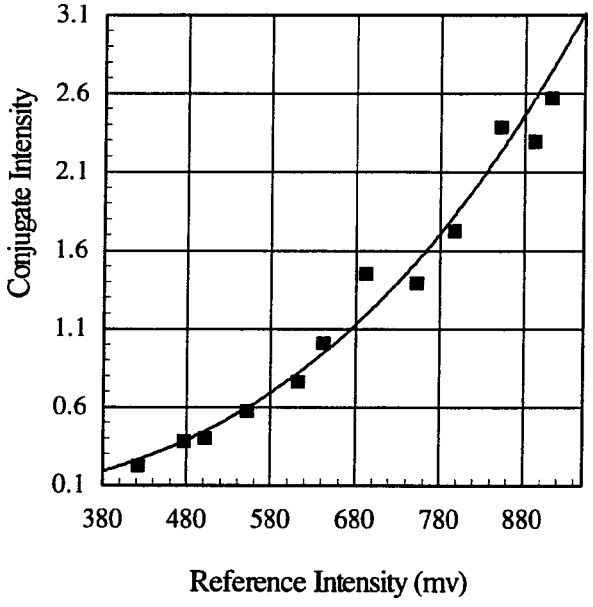

(b)

Figure 4.10 Conjugate signal intensity as a function of laser intensity for complex *cis*-$Mo(CO)_4(PPh_3)_2$. (a) y-axis is the ratio of the conjugate signal intensity over the cube of the reference signal intensity for complex cis-$Mo(CO)_4(PPh_3)_2$. (b) The y-axis is conjugate signal intensity. The power curve ($y = ax^b$) fitting yields b = 3.0376 and r = 0.9864

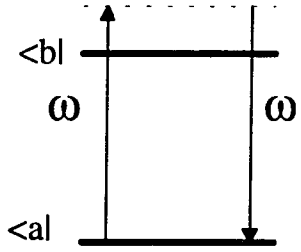

(a) Signal-photon absorption

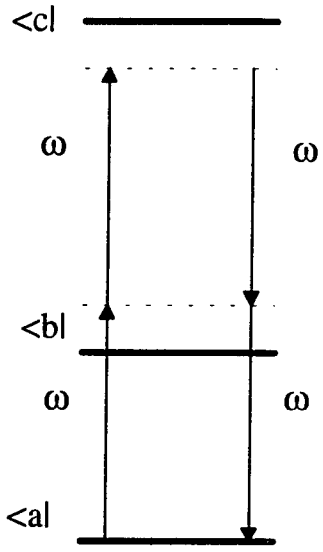

(b) Two-photon absorption

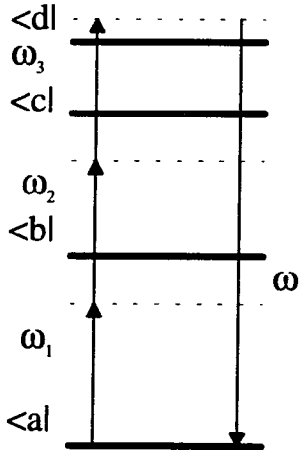

(c) Three-photon absorption

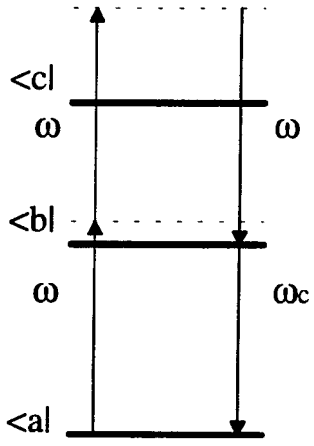

(d) Singly resonance in DFWM

Figure 4.11 Schematics for several types of absorption in a medium. Block lines are the actual energy levels for the medium, and dashed lines are the photon energy

the nonlinear harmonic generations and usually does not happen in the degenerate four-wave mixing process. In the DFWM process, the electron resonant enhancement is most likely due to so called single resonance,[35] which is shown in Figure 4.11 together with the schematics for single- and multi-photon absorption. In Figure 4.11, the dashed line represents the photon energy and the block line is the actual energy level for the molecular system. If the block lines and dashed lines overlap, the resonance occurs. The magnitude of the real part of the $\chi^{(3)}$ tensor element is partially determined by the proximity of the dashed line and the block line, and the sign can be decided from the relative position of the dashed line to the system energy level. The diagrams for two-photon absorption and for degenerate four-wave mixing are similar. The difference between them is that the two-photon absorption involves the imaginary part of the $\chi^{(3)}$ tensor element while the DFWM relies on the real part of the $\chi^{(3)}$ tensor element.

At this time, no exact picture for the energy levels of the samples is available. The measured third-order nonlinear optical value is only valid for the laser frequency used in the experiment and some kind of frequency dispersion for γ value is expected as we can see from the above discussion.

4.6 The Comparison Between DFWM and Z-scan

Because the laser source in our degenerate four-wave mixing has a pulse width of about 20 ns, the contribution from various processes other than the electronic nonlinear response, such as thermal grating and molecular reorientational effect, may influence the measured third-order optical nonlinearity. One way to estimate the magnitude of these effects is to use the z-scan technique.[74] Z-scan has previously been used to measure six of the complexes in this study.[72]

Table 4.4 lists γ values for six molybdenum containing complexes obtained by DFWM and z-scan measurements[72]. It can be seen from the table that there is an excellent agreement between these two groups of the data. This is satisfying, especially when

TABLE 4.4 The Comparisons Between DFWM and Z-scan

	Z-scan	DFWM
Complex	γ/γ_{CS_2}	γ/γ_{CS_2}
cis-$Mo(CO)_4(PPh_3)_2$	1.000	1.866
trans-$Mo(CO)_4(PPh_3)_2$	0.315	0.362
cis-$Mo(CO)_4(PPh_2OMe)_2$	0.056	0.054
cis-$Mo(CO)_4(PPh_2Me)_2$	0.037	0.0044
$Mo(CO)_5(PPh_3)$	0.018	0.002
$Mo(CO)_5(PPh_2NHMe)$	0.011	0.007

considering that DFWM and z-scan are totally different techniques. It should be pointed out that the z-scan experiment utilizes the same laser source as in the DFWM measurements.

Of the possible nonelectronic resonance enhancements, the thermal effect is the first one that needs to be examined. It is expected that thermal enhancement in our samples will be minimal due to low linear absorption at the laser wavelength, as mentioned earlier. This has been verified by the z-scan experiment. The nearly identical valley and peak values for the $\chi^{(3)}$ measurement obtained by the by the z-scan technique show that linear absorption has little effect on the z-scan curve. If the sample solution had absorbed the incident light, the thermal expansion of sample solution would have led to the unequal valley and peak values due to the solution density gradient along the light path within sample.

Another possible nonelectronic enhancement toward the measured γ value is the reorientational response of the medium to the incident optical field. As mentioned in Chapter 3, the molecular reorientational response time for anisotropic liquid is longer than 10^{-12} seconds. At the laser pulse width of nanosecond, it is possible that some reorientational process might contribute toward the measured molecular hyperpolarizabilities. However, the similarity of our γ values for THF and CS_2 to those measured with a pico-second pulse width laser (our measured γ values are 13% larger) suggests that the molecular reorientation contribution is relative insignificant. Thus, we believe that the electronic response is the dominant factor which determines the second-order molecular hyperpolarizability of our samples.

There is a disagreement in the sign of the real part of the γ tensor element between the DFWM and Z-scan measurements. DFWM shows that three of the six complexes in Table 4.3 have possibly a negative real part, while the z-scan yields a positive real part for all six complexes. Because the sign is usually determined by one or two measurements at low concentration in DFWM technique, the weak signal intensity and a relatively large

data uncertainty might have caused a fallacious negative sign. Because the z-scan technique is more reliable in determining the sign for the real part of the γ tensor element according to the energy-z position plot having either a valley-peak or peak-valley shape, it seems that all complexes have a positive real part of their γ tensor elements.

CHAPTER 5

CONCLUSION

A degenerate four-wave mixing experiment apparatus has been built. The light source is a Nd:YAG Pockels' cell Q-switched pulse laser. The output wavelength of the laser is at 1064 nm. After going through a KDP frequency doubler, the light used in DFWM has a wavelength of 532 nm and a power of 7 mJ when the laser is operating at a rate of 2 pps. The variation of the laser intensity is within 3%. The pulse time duration is 20 ns, which is quite long when compared to nonlinear medium's thermal relaxation time. To get rid of the thermal and the molecular reorientation contributions towards the measured $\chi^{(3)}$ value, a pulse width of ps level is desired. A tunable mode-lock dye laser will provide a powerful tool in investigating $\chi^{(3)}$ value's dispersion property as well as distinguishing the resonant effects by tuning laser wavelength into and away from the possible resonant region.

We choose the backward-type degenerate four-way mixing configuration. One of the advantages of this arrangement is avoidance of polarizing two pump waves in a direction other than that of the probe wave to minimize background in the conjugate signal. This is a must in the forward type configuration. However, there is a report that carefully aligned forward type configuration can enhance the third-order nonlinear process via exciting medium electronic states.

Another advantage of the backward-type DFWM is that the phase match condition is more easily satisfied. In the sense of potential applications, like image wavefront correction, the backward configuration measures an effective $\chi^{(3)}$ value that is much closer to the one in the actual applications.

The experiment results have an uncertainty of 26%. The sources of the experiment error are believed to come from the stray light, especially from the nonconjugate reflection of the forward pump beam because of the very small angle between the probe and the forward pump waves. Although a spatial filter system is employed, the optical background is still at about 5 to 20% of the total conjugate signal intensity. The other error sources are the electronic background, the electromagnetic interference from the high voltage driving circuit for the Pockels cell, and the nonuniform spectra of the neutral density filters.

Calibration of the DFWM system is made using carbon disulphide (CS_2) solution. The relative measurement of the third-order susceptibility, $\chi^{(3)}$, for carbon disulphide yields 7.6×10^{-13} esu, which is 13% larger than the reported $\chi^{(3)}$ of CS_2 by the technique of DFWM with a laser pulse width of 20 pS. The difference is believed to be due to our longer laser pulse duration. The thermal effect is not considered to be the major factor in our experiment because the laser wavelength (532 nm) is far away from the nearest linear absorption peak (at about 350 nm). The most possible source of any enhancement other than the pure electronic one is the molecular reorientation. The DFWM technique can not differentiate the pure electronic and the molecular reorientational effects unless a ps laser is utilized.

The measured second-order molecular hyperpolarizabilities for the metal complexes vary from the largest of the order of 10^{-31} esu to the smallest of the order of 10^{-34} esu. The type and the coordination geometry of the ligand have the biggest effect on the third-order optical nonlinearity.

It is widely believed that large third-order nonlinear optical response for an organic material comes from an extended π electron delocalization. A system of long conjugate structure, like conjugate polymer, is thought of the ideal material for this purpose. To extend the possible π-electron delocalization between the ligands, transition metal atoms have been introduced into organic system because of their rich low-lying valence electron

states. Another approach is to coordinate electron donor/acceptor ligands into metal organic system hoping that the resulting electric dipole would enhance medium nonlinear response to the light field.

Good electron donor tends to increase electron density at the transition metal atom, and good electron acceptor will withdraw electron density from the transition metal. This charge transfer induces a larger electric dipole momentum. According the theory based on the bonded charge anharmonic oscillator model, large electric dipole will yield a stronger nonlinear response. Ligands, such as Me, are good electron-donors to the phosphorous atom.

However, the experimental results do not support the hypothesis above. Although the cis-type coordination geometry of the bis(phosphine) Mo complex yields a larger γ value than does the trans- type, which is believed to be attributed to the electric dipole momentum within the molecule, the enhancement to the measured γ value due to the electric dipole within complexes is small when compared to that due to the substituents on ligand. Furthermore, mono-phosphine complexes have the γ values that are about the same as compounds PPh_3 and $OPPh_3$ have. It has been observed also that although bis(phosphine) molybdenum complexes possess large second-order molecular hyperpolarizabilities, either electron donor or acceptor groups on the phosphine ligands do not make much difference in the measured γ values.

The molecular hyperpolarizabilities for molybdenum complexes increase rapidly as the number of π-electron structure groups, such as phenyl and thiophene, and other π-electron structures, like C = O and $p\pi$-$d\pi$ orbitals of nitrogen between the phosphorus and the nitrogen, in the ligands increase. The more substituents with a conjugated structure attached to the phosphorous atom, the larger the third-order nonlinear susceptibility will be. A power fitting of that relationship results a relationship:

$$\gamma = 3.5351 \times 10^{-36} \cdot N^{4.9985}, \qquad (5.1)$$

with N being the number of π electron structures in the ligands. The regression coefficient r is 0.9706. This power relation is very similar to that reported for thiophine oligomers. It should be pointed out that thiophine oligomer has a linear conjugated π electron structure where the loosely bonded π electrons can move freely over the entire molecule. This similarity suggests that the π electrons in phenyl groups respond to the incident laser light like free-moving electrons.

From our experiment results, the type of the transition metal does affect the measured γ values. It seems that complexes of second-row transition metals (Mo) exhibit a larger γ value than those of third-row elements. However, from the fact that mono-substitution of CO by a phosphine ligand does not change γ values at all, it is unlikely that π electrons in the ligands actually delocalize over the entire molecular structure. The transition metal atoms in bis(phosphine) complexes act more likely to enhance the electric dipole momentum instead of being a "bridge" between ligands to provide the path for the possible ligand-metal-ligand π-electron delocalization.

Although the functions of the transition metal atoms in our samples are not exactly known, one of them might be to allow more charge transfer between the neighboring ligands, which is especially true for the cis-type complexes. The measured γ values are many times larger than the simple summation of that of the conjugated groups in the ligands. Thus, the ligand-ligand coupling, both π-electron coupling and σ-electron coupling, in addition to the increased electric dipole momentum, may be the major source of enhancing the samples' third-order nonlinear optical property.

Based on the experimental results, further investigations are needed to study the origins of the third-order optical nonlinearity for the Mo complexes. It will be interesting to look at complexes $Mo(CO)_{6-n}(phosophine)_n$ with the integer n being 3 or larger. If what we have found can be extended to the complexes with a bigger number of phosphine ligands, the γ values of those complexes will be very large. Other approaches would be coordinating some π-electron structures onto the phosphine ligands to make the ligands

more conjugated, and replacing Mo with metals of better electron acceptor ability. Of course, a laser of a shorter pulse duration is always desired to avoid possible nonelectronic processes.

REFERENCES

1. P.A. Franken, A.E. Hill, W. Peter and G. Weinreich, Phys. Rev. Lett. **7**, 118, (1961)

2. G.D. Boyd, R.C. Miller, K. Nassau, W.L. Bond and A. Savage, Appl. Phys. Lett. **5**, 234 (1964)

3. W. Kaiser and C.G.B. Garrett, Phys. Rev. Lett. **7**, 229 (1961)

4. Y.R. Shen and N. Bloemberg, Phys. Rev. **137**, A1787 (1965)

5. C.C. Wang and G.W. Racette, Appl. Phys. Lett. **6**, 169 (1965)

6. R.W. Minck, R.W. Terhune and C.C. Wang, Appl. Optics **5**, 1595 (1966)

7. N. Bloemberg, "Nonlinear Optics," Benjamin, New York, 1965

8. S.M. Jensen, IEEE J. Quant. Electron. **QE-18**, 1580 (1982)

9. H.M. Gibbs, "Optical Bistability: Controlling Light with Light," Academic, Orlando, 1985, p 35

10. H.G.Winful, J.H. Marburger and E. Garmine, Appl. Phys. Lett. **35**, 379 (1979)

11. A. Yariv and R.A. Fisher, "Optical Phase Conjugation," Edited by R.A. Fisher, Academic, New York, 1983, Ch.1, Ch. 2

12. M.J. Soileau, W.E. Williams and E.W. Stryland, IEEE J. Quant. Electron. **QE-19**, 731 (1983)

13. B.G. Kushner, et al., "Nonlinear Optical Properties of Polymers, Materials Research Society Symposium Procedings," **109**, Materials Research Society, Pittsburgh, 1988, p 3

14. J.A. Amstrong, N. Bloembergen, I. Ducing and P.S. Pershan, Phys. Rev. **127**, 1918 (1962)

15. N. Bloembergen and Y.R. Shen, Phys. Rev. **133**, A37 (1964)

16. C.K.N. Patel, R.E. Slusher and P.A. Fleury, Phys. Rev. Lett. **17**, 1011 (1966)

17. D.A.B. Miller, S.D. Smith and B.S. Wherrett, Opt. Commun. **32**, 221 (1980)

18. H.S. Nalwa, Appl. Organometallic Chem. **5**, 349 (1991)

19. J.P. Hermann, Opt. Commun. **9** , 74 (1973)

20. K.C. Rustagi and J. Ducuing, Opt. Commun. **10**, 258 (1974)

21. D. Ulrich, SPIE **1104**, 201 (1989)

22. C.D. Gutsche and D.J. Pasto, "Fundamentals of Organic Chemistry," Prentice Hall, Englewood Cliffs, 1975, Ch. 1

23. G.P. Agnawal, C. Cojon and C. Flytzasnis, Phys. Rev. **B17**, 776 (1978)

24. M.T. Zhao, M. Samoc, B.P. Singh and P.N. Prasad, J. Phys. Chem. **93**, 7916 (1978)

25. S.A. Jenckle, W.C. Chen, S. Lo and S.R. Flom, Appl. Phys. Lett. **57**, 126 (1990)

26. D.C. Rodenberger, J.R. Heflin and A.F. Garito, Lett. to Nature **359**, 309 (1992)

27. C. Elschenbroich and A. Salzer, "Organometallics: a Concise Introduction," VCH, New York, 1992, Ch. 12

28. S.N. Oliver, C.S. Winter, J.D. Rush, A.E. Underhill and C. Hill, SPIE Proc. **1337**, 81 (1990)

29. J.R. Lindle, J.S. Shirk, et al., "Proc. Symp. on New Materials for Nonlinear Optics," Amer. Chem. Society Symp. Proc. **20**, 1991

30. D.R. Ulrich, Mol. Cryst. Liq. Cryst. **189**, 3 (1990)

31. A.F. Garito, and J.W. Wu, SPIE Proc. **1147**, 2 (1989)

32. J.D. Jackson, "Classic Electrodynamics," Wiley, New York, 1975, p 136

33. J.F. Reintjes, "Nonlinear Optical Parametric Process in Liquida and Gases," Academic, New York, 1984, p 11

34. H.A. Bethe and R.W. Jackiw, "Intermediate Quantum mechanics," Benjamin, Menlo Park, 1986, p 63, p 288

35. Y.R. Shen, "The Principles of Nonlineatr Optics," Wiley, New York, 1984, Ch. 1, p 16, p 95, Ch. 14

36. Y. Prior, IEEE J. Quant. Electron. **QE-20**, 37 (1984)

37. P.L. Knight, "The Elements of Nonlinear Optics," Cambridge, New York, 1990, Ch. 5

38. C. Flytzanis and J. Ducuing, Phys. Rev. **178**, 1218 (1969)

39. J.L. Pariser and R.G. Parr, J. Chem. Phys. **21**, 466 (1953)

40. J.A. Pople, Trans. Fraday Soc. **49**, 1375 (1953)

41. P.N. Prasad and D.J. Williams, "Introdection to Nonlinear Optical Effects in Molecules and Polymers," Wiley, New York, 1990, Ch. 4, p 220, p 274

42. F.A. Hopf, A. Tomita, K.H. Womack and J.L. Jewell, J. Opt. Soc. Am. **69**, 968 (1979)

43. J.B. Marion and M.A. Heald, "Classic Electrmagnetic Radiation," Academic, New York, Ch. 11

44. G.M. Gray, Inorganica Chimica Acta **81**, 157 (1984)

45. R.G. Caro and M.C. Gower, IEEE J. Quant. Electro. **QE-18**, 1376 (1982)

46. E. Kajar and J. Messier, Phys. Rev. **A32**, 2352 (1985)

47. P.N. Prasad, "Nonlinear Optical and Electroactive Polymers," Plenum, New York, 1988, p 41

48. S. Ghosal, M. Samoc, P.N. Prasad and J.J. Tufariello, J. Phys. Chem. **94**, 2849 (1990)

49. Aldrich Catalog, Aldrich Co., 1988

50. B.A. Reinhardt, et al., Chem. Mater. **3**, 258 (1991)

51. M. Zhao, et al., Chem. Mater. **2**, 670 (1990)

52. D.V.G.L., N. Rao, F.J. Aranda, J.F. Roach, and D.E. Remy, Appl. Phys. Lett. **58**, 1241 (1991)

53. J.S. Shirk, J.R. Lindle, F.J. Bartoli, and M.E. Boyle, J. Phys. Chem. **96**, 5847 (1992)

54. A.K. Agrawal, S.A. Jenekhe, H. Vanherzeele, and J.S. Meth, J. Phys. Chem. **96**, 2837 (1992)

55. D. Li, T.J. Marks, and M.A. Ratner, J. Phys. Chem. **96**, 4325 (1992)

56. B.A. Reinhardt, TRIP **1**, 4 (1993)

57. D.S. Chemla, "Nonlinear Optics: Materials and Devices," (C. Flytzanis and J.L. Oudar, eds.), Springer, 1986

58. M.T. Zhao, B.P. Singh and P.N. Prasad, Phys. Chem. **89**, 5535 (1988)

59. C.K.N. Patel, R.E. Slusher and P.A. Fleury, Phys. Rev. Lett. **17**, 1011 (1966)

60. D.E Watkins, J.F. Figweira and S.J. Thomas, Opt. Lett. **5**, 169 (1980)

61. D.A.B. Miller, S.D. Smith and B.S. Wherrett, Opt. Commun. **35**, 221 (1980)

62. J.W. Box and G.M. Gray, Inor. Chem. **26**, 2774 (1987)

63. J.W. Box and G.M. Gray, Magn. Res. Chem. **24**, 527 (1986)

64. G.M. Gray and C.S. Kraihanzel, Inor. Chem. **22**, 2959 (1983)

65. G.M. Gray, Inor Chimica Acta **116**, 21 (1986)

66. G.M. Gray, R.J. Gray and D.C. Berndt, J. Magn. Res. **57**, 347 (1984)

67. G.M. Gray, J.E. Whitter and J.W. Box, Inor. Chemica Acta **120**, 25 (1986)

68. J.A. Osaheni, S.A. jenekhe ans H. Vanbergeele, J. Phys. Chem. **96**, 2830 (1992)

69. M.T. Zhao, B.P. Singh, and P.N. Prasad, J. Chem. Phys. **89**, 5535 (1988)

70. M.T. Zhao, M. Smoc, and P.N. Prasad, J. Chem. Phys. **93**, 7916 (1989)

71. L.T. Cheng, M. Tam and G.R. Meredith, Mol. Cryst. Liq. Cryst. **189**, 137 (1990)

72. G. Burgess, Master Thesis, The University of Alabama at Birmingham, Birmingham, 1993

73. M.K. Casstevens, M. Samoc, J. Pfloger and P.N. Prasad, J. Chem. Phys. **92**, 2019 (1990)

74. M. Sheik-Bahae, A.A. Said, E.W. van Stryland, Opt. Lett. **14**, 955 (1989)

75. J.A. Pople, D.P.Santry and G.A. Segal, J. Chem. Phys. **43**, S129 (1965)

76. J.A. Pople, D.L. Beveridge and P.A. Dobosh, J. Chem. Phys. **47**, 2026 (1967)

77. N.C. Baird and M.J.S. Dewar, J. Chem. Phys. **50**, 1262 (1969)

78. J. Wilson and J.F.B. Hawkes, "Optoelectronics: An Introduction," Prentice-Hall, Inc., Englewood Cliffs., New Jersey, 1983, p 358

79. B.I. Davydov, I.D. Derkachiva, V.V. Dunina, M.E. Zhabotinskii, V.F. Zolin, L.G. Koreneva, and M.A. Samokhina, Sov. Phys. JEPT. Lett. **12**, 16 (1970)

80. G. Gray, et al. Chemistry Department, UAB, Birmingham, Al., private communication

81. G. Arfken, "Mathematical Methods for Physicists," Academic, Orlando, Florida, 1985, p 798

GRADUATE SCHOOL
UNIVERSITY OF ALABAMA AT BIRMINGHAM
DISSERTATION APPROVAL FORM

Name of Candidate Tianyi Zhai

Major Subject Physics

Title of Dissertation A Degenerate Four-Wave Mixing Study of Third-Order Optical Nonlinearity of Transition Metal-Containing Organic Complexes

Dissertation Committee:

Christopher Lawson , Chairman

Gary Gray

Joseph Harrison

Jimmy Mays

John Young

Director of Graduate Program

Dean, UAB Graduate School

Date 4/7/94